EUROPEAN ORGANIZATION FOR NUCLEAR RESEARCH (CERN)

CERN-PH-EP-2015-279
LHCb-PAPER-2015-046
20th October 2015

arXiv:1510.05949v2 [hep-ex] 12 Jul 2016

Production of associated Υ and open charm hadrons in pp collisions at $\sqrt{s} = 7$ and 8 TeV via double parton scattering

The LHCb collaboration[†]

Abstract

Associated production of bottomonia and open charm hadrons in pp collisions at $\sqrt{s} = 7$ and 8 TeV is observed using data corresponding to an integrated luminosity of $3\,\text{fb}^{-1}$ accumulated with the LHCb detector. The observation of five combinations, $\Upsilon(1S)D^0$, $\Upsilon(2S)D^0$, $\Upsilon(1S)D^+$, $\Upsilon(2S)D^+$ and $\Upsilon(1S)D_s^+$, is reported. Production cross-sections are measured for $\Upsilon(1S)D^0$ and $\Upsilon(1S)D^+$ pairs in the forward region. The measured cross-sections and the differential distributions indicate the dominance of double parton scattering as the main production mechanism.

Published in JHEP 07 (2016) 052

© CERN on behalf of the LHCb collaboration, licence CC-BY-4.0.

[†]Authors are listed at the end of this paper.

1 Introduction

Production of multiple heavy quark pairs in high-energy hadron collisions was first observed in 1982 by the NA3 collaboration in the channels $\pi^-(\mathrm{p})\,\mathrm{nucleon} \to \mathrm{J/\psi\,J/\psi} + \mathrm{X}$ [1, 2]. Soon after, evidence for the associated production of four open charm particles in pion-nucleon reactions was obtained by the WA75 collaboration [3]. A measurement of J/ψ pair production in proton-proton (pp) collisions at $\sqrt{s} = 7\,\mathrm{TeV}$ [4] has been made by the LHCb collaboration in 2011. This measurement appears to be in good agreement with two models within the single parton scattering (SPS) mechanism, namely non-relativistic quantum chromodynamics (NRQCD) calculations [5] and k_T-factorization [6]. However the obtained result also agrees with predictions [7] of the double parton scattering (DPS) mechanism [8–12].

The production of J/ψ pairs has also been observed by the D0 [13] and CMS [14] collaborations. A large double charm production cross-section involving open charm in pp collisions at $\sqrt{s} = 7\,\mathrm{TeV}$ has been observed by the LHCb collaboration [15]. The measured cross-sections exceed the SPS expectations significantly [16–20] and agree with the DPS estimates. A study of differential distributions supports a large role for the DPS mechanism in multiple production of heavy quarks.

The study of $(\mathrm{b\bar{b}})(\mathrm{c\bar{c}})$ production in hadronic collisions started with the observation of $\mathrm{B_c^+}$ mesons in $\mathrm{p\overline{p}}$ collisions by the CDF collaboration [21]. A detailed study of $\mathrm{B_c^+}$ production spectra in pp collisions by the LHCb collaboration [22] showed good agreement with leading-order NRQCD calculations [23–25] including the SPS contribution only.

The leading-order NRQCD calculations using the same matrix element as in Ref. [23], applied to another class of $(\mathrm{b\bar{b}})(\mathrm{c\bar{c}})$ production, namely associated production of bottomonia and open charm hadrons in the forward region, defined in terms of the rapidity y as $2 < y < 4.5$, predict [26]

$$R_\mathrm{SPS} = \frac{\sigma^{\Upsilon \mathrm{c\bar{c}}}}{\sigma^{\Upsilon}} = (0.2 - 0.6)\,\%\,, \tag{1}$$

where $\sigma^{\Upsilon \mathrm{c\bar{c}}}$ denotes the production cross-section for associated production of $\Upsilon \mathrm{c\bar{c}}$-pair and σ^{Υ} denotes the inclusive production cross-section of Υ mesons. A slightly smaller value of R_SPS is obtained through the k_T-factorization approach [17, 27–31] using the transverse momentum dependent gluon density from Refs. [32–34],

$$R_\mathrm{SPS} = \frac{\sigma^{\Upsilon \mathrm{c\bar{c}}}}{\sigma^{\Upsilon}} = (0.1 - 0.3)\,\%\,. \tag{2}$$

Within the DPS mechanism, the Υ meson and $\mathrm{c\bar{c}}$-pair are produced independently in different partonic interactions. Neglecting the parton correlations in the proton, the contribution of this mechanism is estimated according to the formula [35–37]

$$\sigma^{\Upsilon \mathrm{c\bar{c}}} = \frac{\sigma^{\Upsilon} \times \sigma^{\mathrm{c\bar{c}}}}{\sigma_\mathrm{eff}}\,, \tag{3}$$

where $\sigma^{\mathrm{c\bar{c}}}$ and σ^{Υ} are the inclusive charm and Υ cross-sections, and σ_eff is an effective cross-section, which provides the proper normalization of the DPS cross-section estimate.

The latter is related to the transverse overlap function between partons in the proton. Equation (3) can be used to calculate the ratio $R_{\rm DPS}$ as

$$R_{\rm DPS} = \frac{\sigma^{\Upsilon c\bar{c}}}{\sigma^{\Upsilon}} = \frac{\sigma^{c\bar{c}}}{\sigma_{\rm eff}}. \tag{4}$$

Using the measured production cross-section for inclusive charm in pp collisions at the centre-of-mass energy 7 TeV [38] in the forward region and $\sigma_{\rm eff} \sim 14.5\,{\rm mb}$ [39, 40], one obtains $R_{\rm DPS} \sim 10\%$, which is significantly larger than $R_{\rm SPS}$ from Eq. (1). The production cross-sections for $\Upsilon(1S)D^0$ and $\Upsilon(1S)D^+$ at $\sqrt{s} = 7\,{\rm TeV}$ are calculated using the measured prompt charm production cross-section from Ref. [38] and the $\Upsilon(1S)$ cross-section from Ref. [41]. In the LHCb kinematic region, covering transverse momenta $p_{\rm T}$ and rapidity y of $\Upsilon(1S)$ and $D^{0,+}$ mesons of $p_{\rm T}(\Upsilon(1S)) < 15\,{\rm GeV}/c$, $1 < p_{\rm T}(D^{0,+}) < 20\,{\rm GeV}/c$, $2.0 < y(\Upsilon(1S)) < 4.5$ and $2.0 < y(D^{0,+}) < 4.5$, the expected production cross-sections are

$$\mathscr{B}_{\mu^+\mu^-} \times \sigma^{\Upsilon(1S)D^0}_{\sqrt{s}=7\,{\rm TeV}}\Big|_{\rm DPS} = 206 \pm 17\,{\rm pb}, \tag{5a}$$

$$\mathscr{B}_{\mu^+\mu^-} \times \sigma^{\Upsilon(1S)D^+}_{\sqrt{s}=7\,{\rm TeV}}\Big|_{\rm DPS} = 86 \pm 10\,{\rm pb}, \tag{5b}$$

where $\mathscr{B}_{\mu^+\mu^-}$ is the branching fraction of $\Upsilon(1S) \to \mu^+\mu^-$ [42], $\sigma_{\rm eff} = 14.5\,{\rm mb}$ is used with no associated uncertainty included [39, 40]. The basic DPS formula, Eq. (3), leads to the following predictions for the ratios of production cross-sections R^{D^0/D^+} and $R_{\rm C}^{\Upsilon(2S)/\Upsilon(1S)}$

$$R^{D^0/D^+} = \frac{\sigma^{\Upsilon D^0}}{\sigma^{\Upsilon D^+}} = \frac{\sigma^{D^0}}{\sigma^{D^+}} = 2.41 \pm 0.18\,, \tag{6a}$$

$$R_{\rm C}^{\Upsilon(2S)/\Upsilon(1S)} = \mathscr{B}_{2/1}\frac{\sigma^{\Upsilon(2S)D^0}}{\sigma^{\Upsilon(1S)D^0}} = \mathscr{B}_{2/1}\frac{\sigma^{\Upsilon(2S)D^+}}{\sigma^{\Upsilon(1S)D^+}} = \mathscr{B}_{2/1}\frac{\sigma^{\Upsilon(2S)}}{\sigma^{\Upsilon(1S)}} = 0.249 \pm 0.033\,, \tag{6b}$$

where σ^{D^0}, σ^{D^+} and σ^{Υ} stand for the measured production cross-sections of D^0, D^+ and Υ mesons [38, 41], and $\mathscr{B}_{2/1}$ is the ratio of dimuon branching fractions of $\Upsilon(2S)$ and $\Upsilon(1S)$ mesons.

Here we report the first observation of associated production of bottomonia and open charm hadrons. The production cross-sections and the differential distributions are measured. The latter provide crucial information for understanding the production mechanism. The analysis is performed using the Run 1 data set recorded by the LHCb detector, consisting of $1\,{\rm fb}^{-1}$ of integrated luminosity accumulated at $\sqrt{s} = 7\,{\rm TeV}$ and $2\,{\rm fb}^{-1}$ accumulated at 8 TeV.

2 Detector and data sample

The LHCb detector [43,44] is a single-arm forward spectrometer covering the pseudorapidity range $2 < \eta < 5$, designed for the study of particles containing b or c quarks. The detector includes a high-precision tracking system consisting of a silicon-strip vertex detector

surrounding the pp interaction region, a large-area silicon-strip detector located upstream of a dipole magnet with a bending power of about 4 Tm, and three stations of silicon-strip detectors and straw drift tubes placed downstream of the magnet. The tracking system provides a measurement of the momentum, p, of charged particles with a relative uncertainty that varies from 0.5% at low momentum to 1.0% at 200 GeV/c. The minimum distance of a track to a primary vertex, the impact parameter, is measured with a resolution of $(15 + 29/p_{\rm T})\,\mu$m, where $p_{\rm T}$ is the component of the momentum transverse to the beam, in GeV/c. Different types of charged hadrons are distinguished using information from two ring-imaging Cherenkov detectors. Photons, electrons and hadrons are identified by a calorimeter system consisting of scintillating-pad and preshower detectors, an electromagnetic calorimeter and a hadronic calorimeter. Muons are identified by a system composed of alternating layers of iron and multiwire proportional chambers. The online event selection is performed by a trigger [45], which consists of a hardware stage, based on information from the calorimeter and muon systems, followed by a software stage, which applies a full event reconstruction. At the hardware stage, events for this analysis are selected requiring dimuon candidates with a product of their transverse momenta $p_{\rm T}$ larger than $1.7\,(2.6)\,{\rm GeV}^2/c^2$ for data collected at $\sqrt{s} = 7\,(8)$ TeV. In the subsequent software trigger, two well reconstructed tracks are required to have hits in the muon system, to have $p_{\rm T} > 500\,{\rm MeV}/c$ and $p > 6\,{\rm GeV}/c$ and to form a common vertex. Only events with a dimuon candidate with a mass $m_{\mu^+\mu^-}$ larger than $4.7\,{\rm GeV}/c^2$ are retained for further analysis.

The simulation is performed using the LHCb configuration [46] of the Pythia 6 event generator [47]. Decays of hadronic particles are described by EvtGen [48] in which final-state photons are generated using Photos [49]. The interaction of the generated particles with the detector, and its response, are implemented using the Geant4 toolkit [50, 51] as described in Ref. [52].

3 Event selection

The event selection strategy is based on the independent selection of $\Upsilon(1S)$, $\Upsilon(2S)$ and $\Upsilon(3S)$ mesons (jointly referred to by the symbol Υ throughout the paper) and charmed hadrons, namely $\rm D^0$, $\rm D^+$ and $\rm D_s^+$ mesons and Λ_c^+ baryons (jointly referred to by the symbol C herafter) originating from the same pp collision vertex. The Υ candidates are reconstructed via their dimuon decays, and the $\rm D^0 \to K^-\pi^+$, $\rm D^+ \to K^-\pi^+\pi^+$, $\rm D_s^+ \to K^+K^-\pi^+$ and $\Lambda_c^+ \to {\rm pK}^-\pi^+$ decay modes are used for the reconstruction of charm hadrons. Charge conjugate processes are implied throughout the paper. The fiducial region for this analysis is defined in terms of the $p_{\rm T}$ and the rapidity y of Υ and C hadrons to be $p_{\rm T}^{\Upsilon} < 15\,{\rm GeV}/c$, $2.0 < y^{\Upsilon} < 4.5$, $1 < p_{\rm T}^{\mathsf{C}} < 20\,{\rm GeV}/c$ and $2.0 < y^{\mathsf{C}} < 4.5$.

The event selection for $\Upsilon \to \mu^+\mu^-$ candidates follows previous LHCb studies [41], and the selection of C hadrons follows Refs. [15, 53]. Only good quality tracks [54], identified as muons [55], kaons, pions or protons [56] are used in the analysis. A good quality vertex is required for $\Upsilon \to \mu^+\mu^-$, $\rm D^0 \to K^-\pi^+$, $\rm D^+ \to K^-\pi^+\pi^+$, $\rm D_s^+ \to K^+K^-\pi^+$ and

$\Lambda_c^+ \to pK^-\pi^+$ candidates. For $D_s^+ \to K^+K^-\pi^+$ candidates, the mass of the K^+K^- pair is required to be in the region $m_{K^+K^-} < 1.04$ GeV/c^2, which is dominated by the $D_s^+ \to \phi\pi^+$ decay. To suppress combinatorial background the decay time of C hadrons is required to exceed 100 μm/c. Full decay chain fits are applied separately for selected Υ and C candidates [57]. For Υ mesons it is required that the vertex is compatible with one of the reconstructed pp collision vertices. In the case of long-lived charm hadrons, the momentum direction is required to be consistent with the flight direction calculated from the locations of the primary and secondary vertices. The reduced χ^2 of these fits, both $\chi^2_{\rm fit}(\Upsilon)/{\rm ndf}$ and $\chi^2_{\rm fit}(\mathsf{C})/{\rm ndf}$, are required to be less than 5, where ndf is the number of degrees of freedom in the fit. The requirements favour the selection of charm hadrons produced promptly at the pp collision vertex and significantly suppress the feed down from charm hadrons produced in decays of beauty hadrons. The contamination of such C hadrons in the selected sample varies between $(0.4 \pm 0.2)\%$ for D^+ mesons to $(1.5 \pm 0.5)\%$ for Λ_c^+ baryons.

The selected Υ and C candidates are paired to form $\Upsilon\mathsf{C}$ candidates. A global fit to the $\Upsilon\mathsf{C}$ candidates is performed [57], similar to that described above, which requires both hadrons to be consistent with originating from a common vertex. The reduced χ^2 of this fit, $\chi^2_{\rm fit}(\Upsilon\mathsf{C})/{\rm ndf}$, is required to be less than 5. This reduces the background from the pile-up of two independent pp interactions producing separately a Υ meson and C hadron to a negligible level, keeping 100% of the signal Υ mesons and C hadrons from the same primary vertex. The two-dimensional mass distributions for $\Upsilon\mathsf{C}$ pairs after the selection are displayed in Fig. 1.

4 Signal extraction and cross-section determination

The event yields are determined using unbinned extended maximum likelihood fits to the two-dimensional $\Upsilon\mathsf{C}$ mass distributions of the selected candidates. The fit model is a sum of several components, each of which is the product of a dimuon mass distribution, corresponding to an individual Υ state or combinatorial background, and a C candidate mass distribution, corresponding to a C signal or combinatorial background component. The $\Upsilon(1S) \to \mu^+\mu^-$, $\Upsilon(2S) \to \mu^+\mu^-$ and $\Upsilon(3S) \to \mu^+\mu^-$ signals are each modelled by a double-sided Crystal Ball function [4, 58, 59] and referred to as S_Υ in this section. A modified Novosibirsk function [60] (referred to as S_C) is used to describe the $D^0 \to K^-\pi^+$, $D^+ \to K^-\pi^+\pi^+$, $D_s^+ \to K^+K^-\pi^+$ and $\Lambda_c^+ \to pK^-\pi^+$ signals. All shape parameters and signal peak positions are fixed from fits to large inclusive $\Upsilon \to \mu^+\mu^-$ and C hadron data samples. Combinatorial background components $B_{\mu^+\mu^-}$ and B_C are modelled with a product of exponential and polynomial functions

$$B(m) \propto e^{-\beta m} \times \mathcal{P}_n(m), \tag{7}$$

with a slope parameter β and a polynomial function $\mathcal{P}_n$, which is represented as a Bézier sum of basic Bernstein polynomials of order n with non-negative coefficients [61]. For the large yield ΥD^0 and ΥD^+ samples, the second-order polynomials ($n = 2$) are used in the fit, while $n = 1$ is used for the ΥD_s^+ and $\Upsilon\Lambda_c^+$ cases.

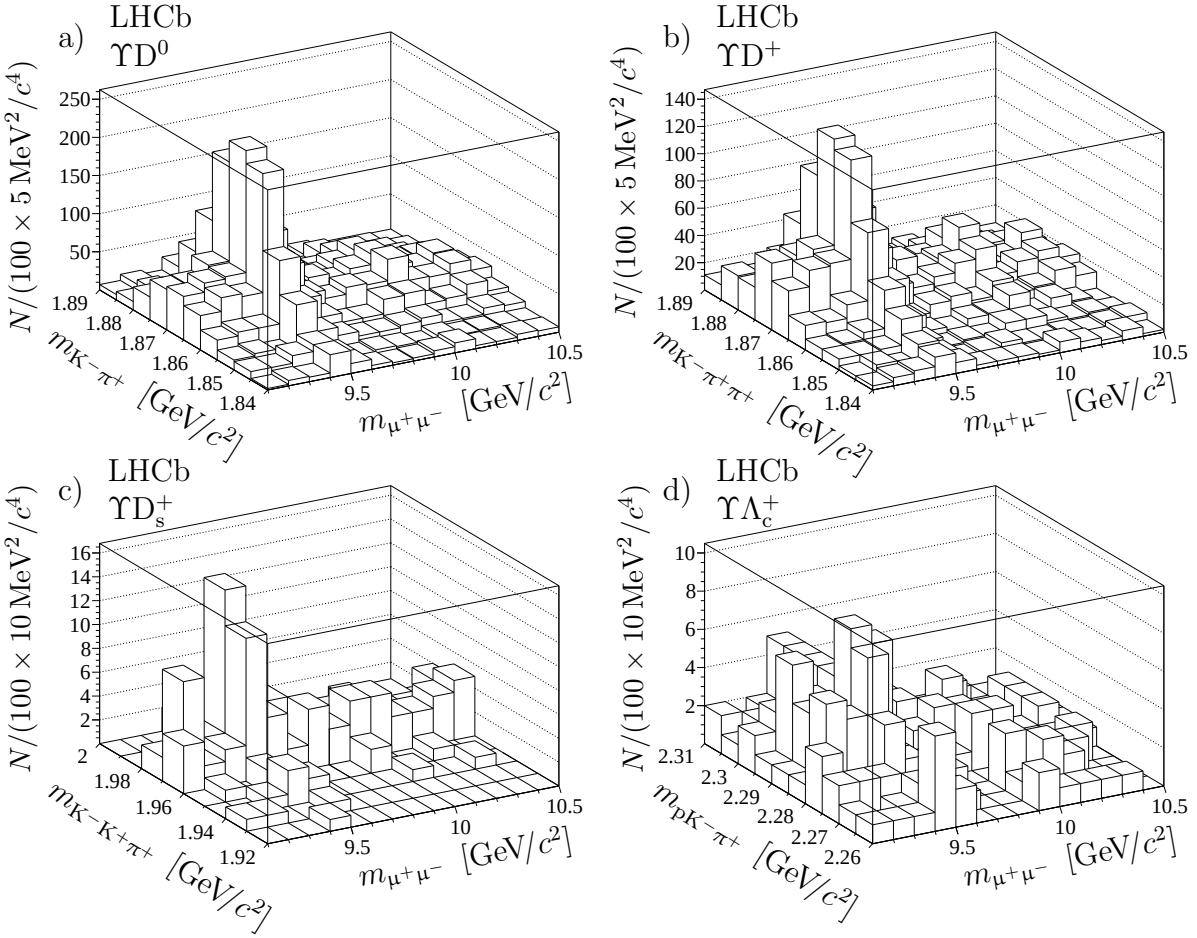

Figure 1: Invariant mass distributions for selected combination of Υ mesons and C hadrons: a) ΥD^0, b) ΥD^+, c) ΥD_s^+ and d) $\Upsilon \Lambda_c^+$.

These basic functions are used to build the components of the two dimensional mass fit following Ref. [15]. For each C hadron the reconstructed signal sample consists of the following components:

- Three ΥC signal components: each is modelled by a product of the individual signal Υ components, $S_{\Upsilon(1S)}(m_{\mu^+\mu^-})$, $S_{\Upsilon(2S)}(m_{\mu^+\mu^-})$ or $S_{\Upsilon(3S)}(m_{\mu^+\mu^-})$, and signal C hadron component, $S_{\mathsf{C}}(m_{\mathsf{C}})$.

- Three components describing the production of single Υ mesons together with combinatorial background for the C signal: each component is modelled by a product of the signal Υ component, $S_{\Upsilon}(m_{\mu^+\mu^-})$ and the background component $B_{\mathsf{C}}(m_{\mathsf{C}})$.

- Single production of C hadrons together with combinatorial background for the Υ component: this is modelled by a product of the signal C component, $S_{\mathsf{C}}(m_{\mathsf{C}})$, and the background component $B_{\mu^+\mu^-}(m_{\mu^+\mu^-})$.

Table 1: Signal yields $N^{\Upsilon\mathsf{C}}$ for $\Upsilon\mathsf{C}$ production, determined with two-dimensional extended unbinned maximum likelihood fits to the candidate $\Upsilon\mathsf{C}$ samples.

	$\Upsilon(1S)$	$\Upsilon(2S)$	$\Upsilon(3S)$
D^0	980 ± 50	184 ± 27	60 ± 22
D^+	556 ± 35	116 ± 20	55 ± 17
D_s^+	31 ± 7	9 ± 5	6 ± 4
Λ_c^+	11 ± 6	1 ± 4	1 ± 3

- Combinatorial background: this is modelled by a product of the individual background components $B_{\mu^+\mu^-}(m_{\mu^+\mu^-})$ and $B_{\mathsf{C}}(m_{\mathsf{C}})$.

For each C hadron the complete fit function $\mathcal{F}(m_{\mu^+\mu^-}, m_{\mathsf{C}})$ is

$$\begin{aligned}\mathcal{F}(m_{\mu^+\mu^-}, m_{\mathsf{C}}) = {} & N^{\Upsilon(1S)\mathsf{C}} \times S_{\Upsilon(1S)}(m_{\mu^+\mu^-}) \times S_{\mathsf{C}}(m_{\mathsf{C}}) \\ & + N^{\Upsilon(2S)\mathsf{C}} \times S_{\Upsilon(2S)}(m_{\mu^+\mu^-}) \times S_{\mathsf{C}}(m_{\mathsf{C}}) \\ & + N^{\Upsilon(3S)\mathsf{C}} \times S_{\Upsilon(3S)}(m_{\mu^+\mu^-}) \times S_{\mathsf{C}}(m_{\mathsf{C}}) \\ & + N^{\Upsilon(1S)B} \times S_{\Upsilon(1S)}(m_{\mu^+\mu^-}) \times B_{\mathsf{C}}(m_{\mathsf{C}}) \\ & + N^{\Upsilon(2S)B} \times S_{\Upsilon(2S)}(m_{\mu^+\mu^-}) \times B_{\mathsf{C}}(m_{\mathsf{C}}) \\ & + N^{\Upsilon(3S)B} \times S_{\Upsilon(3S)}(m_{\mu^+\mu^-}) \times B_{\mathsf{C}}(m_{\mathsf{C}}) \\ & + N^{B\mathsf{C}} \times B_{\mu^+\mu^-}(m_{\mu^+\mu^-}) \times S_{\mathsf{C}}(m_{\mathsf{C}}) \\ & + N^{BB} \times B_{\mu^+\mu^-}(m_{\mu^+\mu^-}) \times B_{\mathsf{C}}(m_{\mathsf{C}}),\end{aligned} \tag{8}$$

where the different coefficients $N^{\Upsilon\mathsf{C}}$, $N^{\Upsilon B}$, $N^{B\mathsf{C}}$ and N^{BB} are the yields of the eight components described above.

The fit results are summarized in Table 1, and the fit projections are presented in Figs. 2, 3, 4 and 5. The statistical significances of the signal components are determined using a Monte-Carlo technique with a large number of pseudoexperiments. They are presented in Table 2. For the five modes, $\Upsilon(1S)D^0$, $\Upsilon(2S)D^0$, $\Upsilon(1S)D^+$, $\Upsilon(2S)D^+$ and $\Upsilon(1S)D_s^+$, the significances exceed five standard deviations. No significant signals are found for the associated production of Υ mesons and Λ_c^+ baryons.

The possible contribution from pile-up events is estimated from data following the method from Refs. [15, 53] by relaxing the requirement on $\chi^2_{\text{fit}}(\Upsilon\mathsf{C})/\text{ndf}$. Due to the requirements $\chi^2_{\text{fit}}(\Upsilon)/\text{ndf} < 5$ and $\chi^2_{\text{fit}}(\mathsf{C})/\text{ndf} < 5$, the value of $\chi^2_{\text{fit}}(\Upsilon\mathsf{C})/\text{ndf}$ does not exceed 5 units for signal events with Υ and C hadron from the same pp collision vertex. The background is subtracted using the *sPlot* technique [63]. The $\chi^2_{\text{fit}}(\Upsilon\mathsf{C})/\text{ndf}$ distributions are shown in Fig. 6. The distributions exhibit two components: the peak at low χ^2 is attributed to associated $\Upsilon\mathsf{C}$ production, and the broad structure at large values of χ^2 corresponds to the contribution from pile-up events. The distributions are fitted with a function that has two components, each described by a Γ-distribution. The shape is

Table 2: Statistical significances of the observed $\Upsilon\mathsf{C}$ signals in units of standard deviations determined using pseudoexperiments. The values in parentheses indicate the statistical significance calculated using Wilks' theorem [62].

	$\Upsilon(1S)$	$\Upsilon(2S)$	$\Upsilon(3S)$
D^0	$> 5\,(26)$	$> 5\,(7.7)$	3.1
D^+	$> 5\,(19)$	$> 5\,(6.4)$	4.0
D_s^+	$> 5\,(6)$	2.5	1.9
Λ_c^+	2.5	0.9	0.9

motivated by the observation that $\chi^2_{\rm fit}/{\rm ndf}$ should follow a scaled-χ^2 distribution. The possible contribution from pile-up events is estimated by integrating the pile-up component in the region $\chi^2_{\rm fit}\left(\Upsilon\mathsf{C}\right)/{\rm ndf} < 5$. It does not exceed 1.5% for all four cases and is neglected.

The production cross-section is determined for the four modes with the largest yield: $\Upsilon(1S)D^0$, $\Upsilon(2S)D^0$, $\Upsilon(1S)D^+$ and $\Upsilon(2S)D^+$. The cross-section is calculated using a subsample of events where the reconstructed Υ candidate is explicitly matched to the dimuon candidate that triggers the event. This requirement reduces signal yields by approximately 20%, but allows a robust determination of trigger efficiencies. The cross-section for the associated production of Υ mesons with C hadrons in the kinematic range of LHCb is calculated as

$$\mathscr{B}_{\mu^+\mu^-} \times \sigma^{\Upsilon\mathsf{C}} = \frac{1}{\mathscr{L} \times \mathscr{B}_{\mathsf{C}}} N^{\Upsilon\mathsf{C}}_{\rm corr}, \tag{9}$$

where $\mathscr{L}$ is the integrated luminosity [64], $\mathscr{B}_{\mu^+\mu^-}$ and $\mathscr{B}_{\mathsf{C}}$ are the world average branching fractions of $\Upsilon \to \mu^+\mu^-$ and the charm decay modes [42], and $N^{\Upsilon\mathsf{C}}_{\rm corr}$ is the efficiency-corrected yield of the signal $\Upsilon\mathsf{C}$ events in the kinematic range of this analysis. Production cross-sections are determined separately for data sets accumulated at $\sqrt{s} = 7$ and 8 TeV.

The efficiency-corrected signal yields $N^{\Upsilon\mathsf{C}}_{\rm corr}$ are determined using an extended unbinned maximum likelihood fit to the weighted two-dimensional invariant mass distributions of the selected $\Upsilon\mathsf{C}$ candidates. The weight ω for each event is calculated as $\omega = 1/\varepsilon^{\rm tot}$, where $\varepsilon^{\rm tot}$ is the total efficiency for the given event.

The effective DPS cross-section and the ratios $R^{\Upsilon\mathsf{C}}$ are calculated as

$$\sigma_{\rm eff} = \frac{\sigma^{\Upsilon} \times \sigma^{\mathsf{C}}}{\sigma^{\Upsilon\mathsf{C}}}, \tag{10a}$$

$$R^{\Upsilon\mathsf{C}} = \frac{\sigma^{\Upsilon\mathsf{C}}}{\sigma^{\Upsilon}}, \tag{10b}$$

where σ^{Υ} is the production cross-section of Υ mesons taken from Ref. [41]. The double-differential production cross-sections of charm mesons has been measured at $\sqrt{s} = 7$ TeV in the region $2.0 < y^{\mathsf{C}} < 4.5$, $p_{\rm T}^{\mathsf{C}} < 8\,{\rm GeV}/c$ [38]. According to FONLL calculations [65–67], the contribution from the region $8 < p_{\rm T}^{\mathsf{C}} < 20\,{\rm GeV}/c$ is significantly smaller than the uncertainty for the measured cross-section in the region $1 < p_{\rm T}^{\mathsf{C}} < 8\,{\rm GeV}/c$. It allows to estimate the production cross-section of charm mesons in the region $2.0 < y^{\mathsf{C}} < 4.5$,

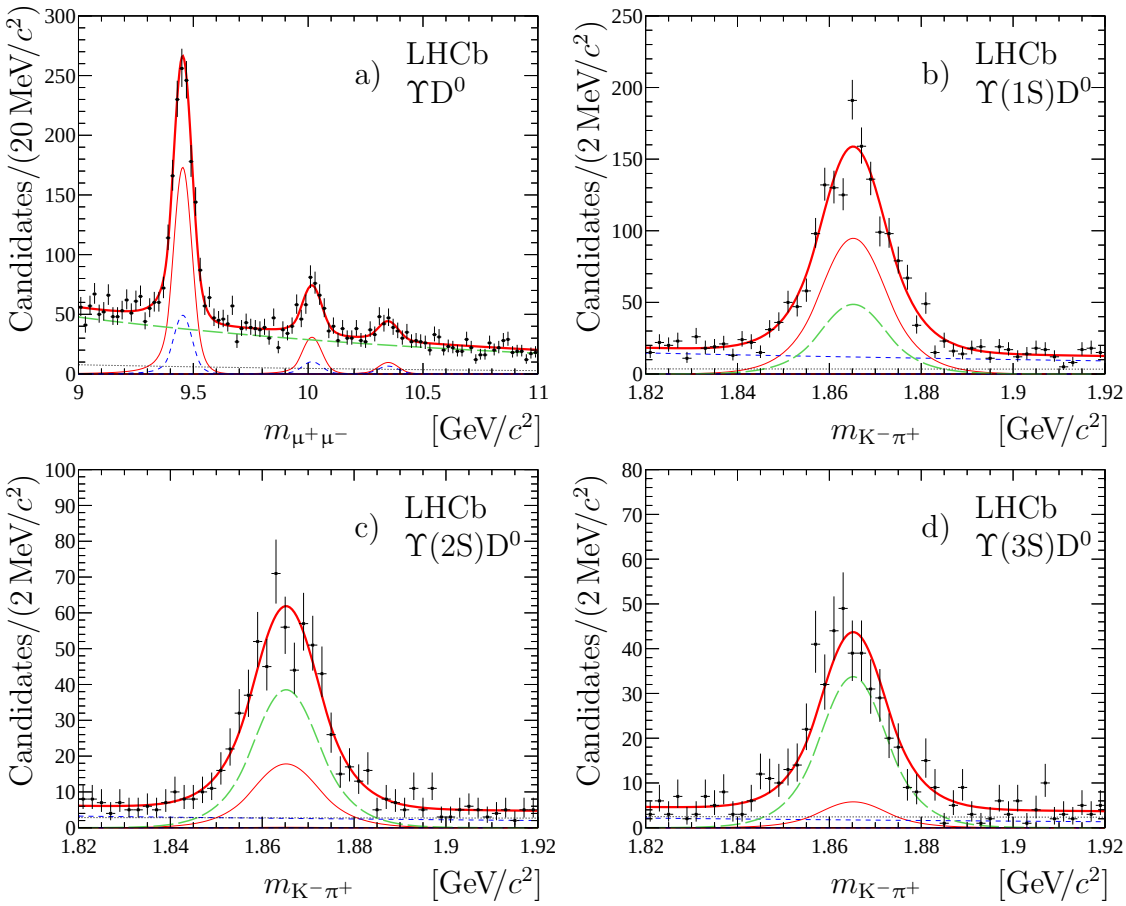

Figure 2: Projections from two-dimensional extended unbinned maximum likelihood fits in bands a) $1.844 < m_{\mathrm{K}^-\pi^+} < 1.887\,\mathrm{MeV}/c^2$, b) $9.332 < m_{\mu^+\mu^-} < 9.575\,\mathrm{GeV}/c^2$, c) $9.889 < m_{\mu^+\mu^-} < 10.145\,\mathrm{GeV}/c^2$ and d) $10.216 < m_{\mu^+\mu^-} < 10.481\,\mathrm{GeV}/c^2$. The total fit function is shown by a solid thick (red) curve; three individual $\Upsilon\mathrm{D}^0$ signal components are shown by solid thin (red) curves; three components describing Υ signals and combinatorial background in $\mathrm{K}^-\pi^+$ mass are shown with short-dashed (blue) curves; the component modelling the true D^0 signal and combinatorial background in $\mu^+\mu^-$ mass is shown with a long-dashed (green) curve and the component describing combinatorial background is shown with a thin dotted (black) line.

$1 < p_{\mathrm{T}}^{\mathsf{C}} < 20\,\mathrm{GeV}/c$, used in Eq. (10a). For the production cross-section of charm mesons at $\sqrt{s} = 8\,\mathrm{TeV}$, the measured cross-section at $\sqrt{s} = 7\,\mathrm{TeV}$ is rescaled by the ratio $R_{8/7}^{\mathrm{FONLL}}(p_{\mathrm{T}}, y)$ of the double-differential cross-sections, as calculated with FONLL [65–67] at $\sqrt{s} = 8$ and $7\,\mathrm{TeV}$.

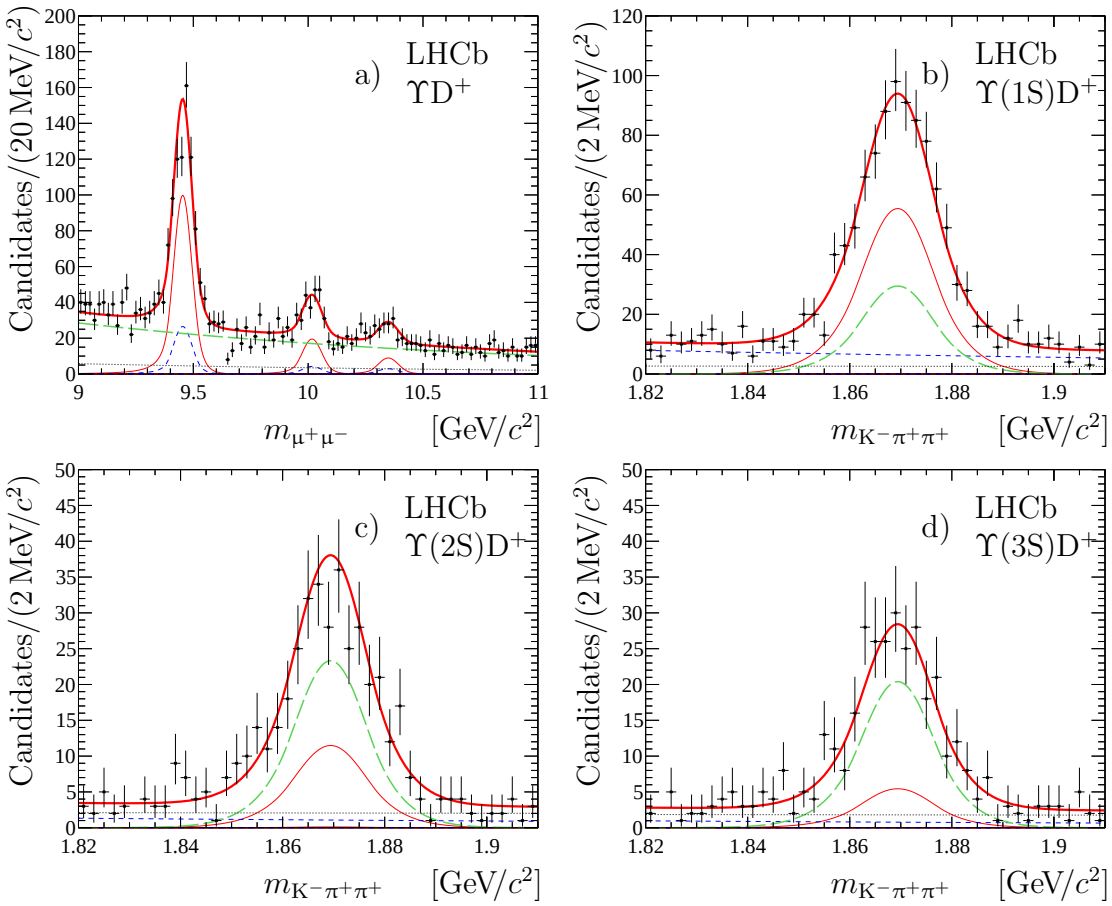

Figure 3: Projections from two-dimensional extended unbinned maximum likelihood fits in bands a) $1.848 < m_{\mathrm{K}^-\pi^+\pi^+} < 1.891\,\mathrm{MeV}/c^2$, b) $9.332 < m_{\mu^+\mu^-} < 9.575\,\mathrm{GeV}/c^2$, c) $9.889 < m_{\mu^+\mu^-} < 10.145\,\mathrm{GeV}/c^2$ and d) $10.216 < m_{\mu^+\mu^-} < 10.481\,\mathrm{GeV}/c^2$. The total fit function is shown by a solid thick (red) curve; three individual $\Upsilon\mathrm{D}^+$ signal components are shown by solid thin (red) curves; three components describing Υ signals and combinatorial background in $\mathrm{K}^-\pi^+\pi^+$ mass are shown with short-dashed (blue) curves; the component modelling the true D^+ signal and combinatorial background in $\mu^+\mu^-$ mass is shown with a long-dashed (green) curve and the component describing combinatorial background is shown with a thin dotted (black) line.

The ratios $R^{\mathrm{D}^0/\mathrm{D}^+}$ and $R_{\mathsf{C}}^{\Upsilon(2\mathrm{S})/\Upsilon(1\mathrm{S})}$, defined in Eq. (6), are calculated as

$$R^{\mathrm{D}^0/\mathrm{D}^+} = \frac{\sigma^{\Upsilon\mathrm{D}^0}}{\sigma^{\Upsilon\mathrm{D}^+}} = \frac{N_{\mathrm{corr}}^{\Upsilon\mathrm{D}^0}}{N_{\mathrm{corr}}^{\Upsilon\mathrm{D}^+}}, \tag{11a}$$

$$R_{\mathsf{C}}^{\Upsilon(2\mathrm{S})/\Upsilon(1\mathrm{S})} = \mathscr{B}_{2/1}\frac{\sigma^{\Upsilon(2\mathrm{S})\mathsf{C}}}{\sigma^{\Upsilon(1\mathrm{S})\mathsf{C}}} = \frac{N^{\Upsilon(2\mathrm{S})\mathsf{C}}}{N^{\Upsilon(1\mathrm{S})\mathsf{C}}} \times \frac{\langle\varepsilon_{\Upsilon(1\mathrm{S})\mathsf{C}}\rangle}{\langle\varepsilon_{\Upsilon(2\mathrm{S})\mathsf{C}}\rangle}, \tag{11b}$$

where $\langle\varepsilon_{\Upsilon\mathsf{C}}\rangle$ denotes the average efficiency. Within the DPS mechanism, the transverse momenta and rapidity spectra of C mesons for the signal $\Upsilon(1\mathrm{S})\mathsf{C}$ and $\Upsilon(2\mathrm{S})\mathsf{C}$ events are expected to be the same. This allows to express the ratio of the average $\langle\varepsilon_{\Upsilon\mathsf{C}}\rangle$ efficiencies

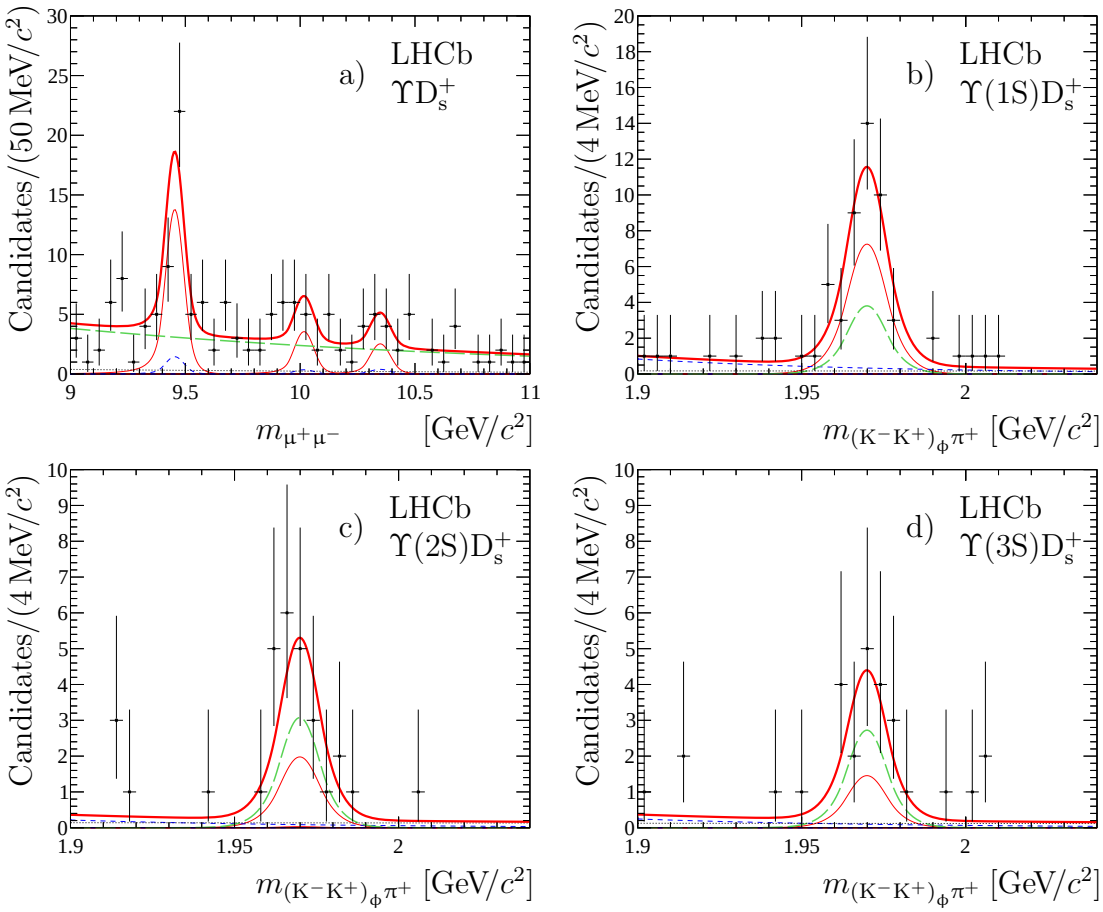

Figure 4: Projections from two-dimensional extended unbinned maximum likelihood fits in bands a) $1.952 < m_{(\mathrm{K^-K^+})_\phi\pi^+} < 1.988\,\mathrm{MeV}/c^2$, b) $9.332 < m_{\mu^+\mu^-} < 9.575\,\mathrm{GeV}/c^2$, c) $9.889 < m_{\mu^+\mu^-} < 10.145\,\mathrm{GeV}/c^2$ and d) $10.216 < m_{\mu^+\mu^-} < 10.481\,\mathrm{GeV}/c^2$. The total fit function is shown by a solid thick (red) curve; three individual ΥD_s^+ signal components are shown by solid thin (red) curves; three components describing Υ signals and combinatorial background in $(\mathrm{K^-K^+})_\phi\,\pi^+$ mass are shown with short-dashed (blue) curves; the component modelling the true D_s^+ signal and combinatorial background in $\mu^+\mu^-$ mass is shown with a long-dashed (green) curve and the component describing combinatorial background is shown with a thin dotted (black) line.

in terms of ratio of average efficiencies for inclusive Υ mesons

$$\frac{\langle\varepsilon_{\Upsilon(1S)\mathsf{C}}\rangle}{\langle\varepsilon_{\Upsilon(2S)\mathsf{C}}\rangle} = \frac{\langle\varepsilon_{\Upsilon(1S)}\rangle}{\langle\varepsilon_{\Upsilon(2S)}\rangle}, \tag{12}$$

and the latter is taken from Ref. [41].

The total efficiency $\varepsilon^{\mathrm{tot}}$, for each $\Upsilon\mathsf{C}$ candidate is calculated following Ref. [15] as

$$\varepsilon^{\mathrm{tot}}_{\Upsilon\mathsf{C}} = \varepsilon^{\mathrm{tot}}_{\Upsilon} \times \varepsilon^{\mathrm{tot}}_{\mathsf{C}}, \tag{13}$$

and applied individually an on event-by-event basis, where $\varepsilon^{\mathrm{tot}}_{\Upsilon}$ and $\varepsilon^{\mathrm{tot}}_{\mathsf{C}}$ are the total

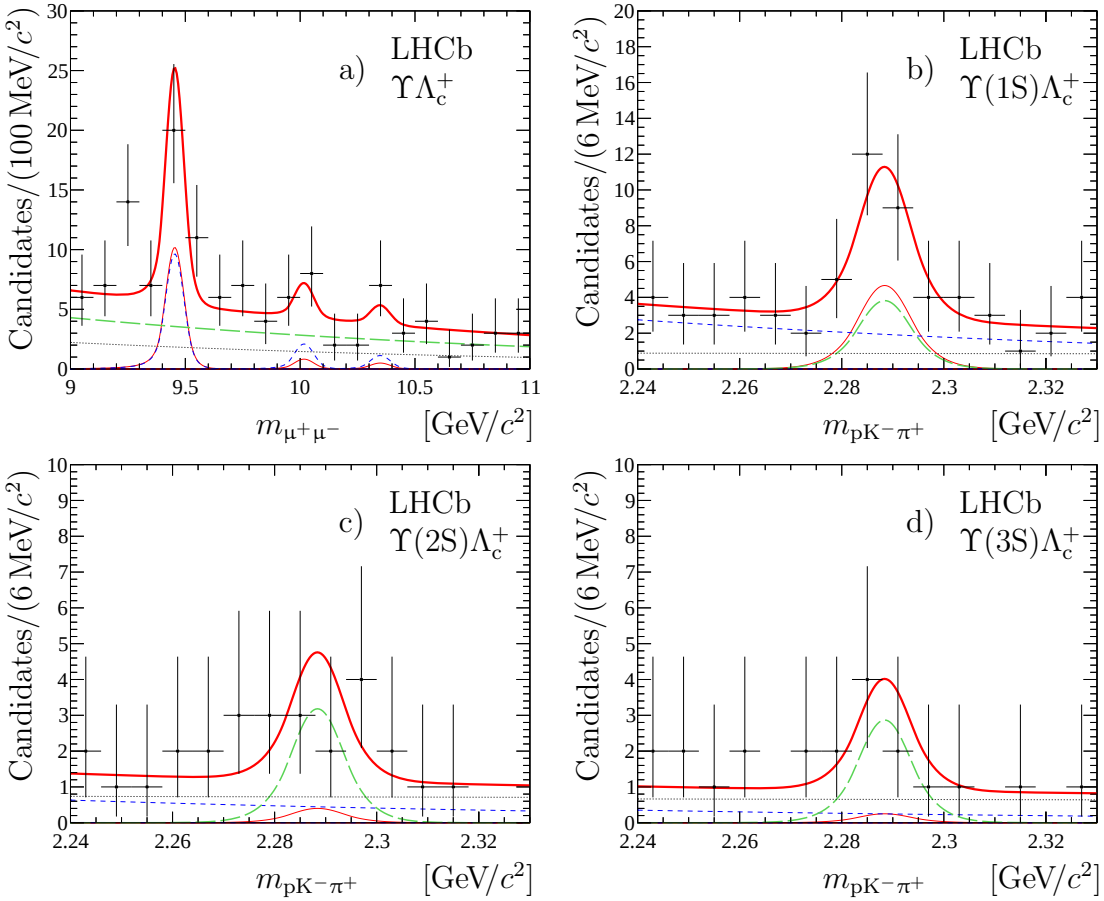

Figure 5: Projections from two-dimensional extended unbinned maximum likelihood fits in bands a) $2.273 < m_{pK^-\pi^+} < 2.304\,\text{MeV}/c^2$, b) $9.332 < m_{\mu^+\mu^-} < 9.575\,\text{GeV}/c^2$, c) $9.889 < m_{\mu^+\mu^-} < 10.145\,\text{GeV}/c^2$ and d) $10.216 < m_{\mu^+\mu^-} < 10.481\,\text{GeV}/c^2$. The total fit function is shown by a solid thick (red) curve; three individual $\Upsilon\Lambda_c^+$ signal components are shown by solid thin (red) curves; three components describing Υ signals and combinatorial background in $pK^-\pi^+$ mass are shown with short-dashed (blue) curves; the component modelling the true Λ_c^+ signal and combinatorial background in $\mu^+\mu^-$ mass is shown with a long-dashed green curve and the component describing combinatorial background is shown with a thin dotted (black) line.

efficiencies for Υ and charm hadrons respectively. These efficiencies are calculated as

$$\varepsilon_\Upsilon^{\text{tot}} = \varepsilon_\Upsilon^{\text{rec}} \times \varepsilon_\Upsilon^{\text{trg}} \times \varepsilon_\Upsilon^{\mu\text{ID}}, \tag{14a}$$

$$\varepsilon_C^{\text{tot}} = \varepsilon_C^{\text{rec}} \times \varepsilon_C^{\text{hID}}, \tag{14b}$$

where ε^{rec} is the detector acceptance, reconstruction and event selection efficiency and ε^{trg} is the trigger efficiency for selected events. The particle identification efficiencies for

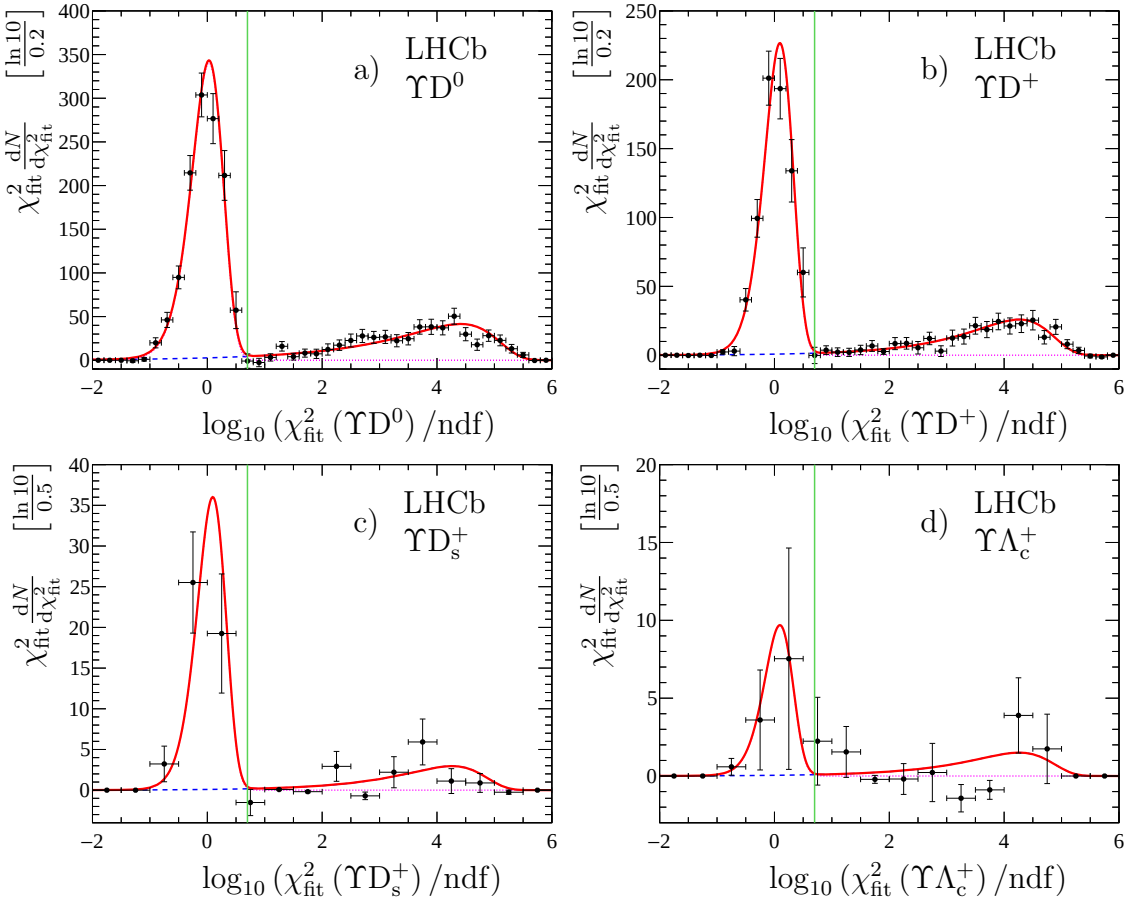

Figure 6: Background-subtracted distributions of $\chi^2_{\rm fit}(\mathsf{C})/{\rm ndf}$ for a) $\Upsilon{\rm D}^0$, b) $\Upsilon{\rm D}^+$, c) $\Upsilon{\rm D}^+_{\rm s}$ and d) $\Upsilon\Lambda^+_{\rm c}$ cases. A thin vertical (green) line indicates the requirement $\chi^2_{\rm fit}(\Upsilon\mathsf{C})/{\rm ndf} < 5$ used in the analysis. The solid (red) curves indicate a fit to a sum of two components, each described by Γ-distribution shape. The pileup component is shown with a dashed (blue) line.

Υ and C candidates $\varepsilon^{\mu{\rm ID}}_{\Upsilon}$ and $\varepsilon^{\rm hID}_{\mathsf{C}}$ are calculated as

$$\varepsilon^{\mu{\rm ID}}_{\Upsilon} = \varepsilon^{\rm ID}_{\mu^+} \times \varepsilon^{\rm ID}_{\mu^-}, \tag{15a}$$

$$\varepsilon^{\rm hID}_{\mathsf{C}} = \prod_{\rm K} \varepsilon^{\rm ID}_{\rm K} \times \prod_{\pi} \varepsilon^{\rm ID}_{\pi} \tag{15b}$$

where $\varepsilon^{\rm ID}_{\mu^\pm}$, $\varepsilon^{\rm ID}_{\rm K}$ and $\varepsilon^{\rm ID}_{\pi}$ are the efficiencies for the single muon, kaon and pion identification, respectively.

The efficiencies $\varepsilon^{\rm rec}$ and $\varepsilon^{\rm trg}$ are determined using simulated samples of Υ, $\rm D^0$ and $\rm D^+$ events as a function of $p_{\rm T}$ and y of the Υ and the C hadron. The differential treatment results in a robust determination of the efficiency-corrected signal yields, with no dependence on the particle spectra in the simulated samples. The derived values of the efficiencies are corrected to account for small discrepancies in the detector response between data and simulation. These corrections are obtained using data-driven techniques [54, 55].

The efficiencies for muon, kaon and pion identification are determined directly from data using large samples of low-background $J/\psi \to \mu^+\mu^-$ and $D^{*+} \to (D^0 \to K^-\pi^+)\,\pi^+$ decays. The identification efficiencies are evaluated as a function of the kinematic parameters of the final-state particles, and the track multiplicity in the event [56].

The efficiency is dependent on the polarisation of the Υ mesons [41, 59, 68, 69] The polarisation of the Υ mesons produced in pp collisions at $\sqrt{s} = 7\,\text{TeV}$ at high p_{T}^{Υ} and central rapidity has been studied by the CMS collaboration [70] in the centre-of-mass helicity, Collins-Soper [71] and the perpendicular helicity frames. No evidence of significant transverse or longitudinal polarisation has been observed for the region $10 < p_{\text{T}}^{\Upsilon} < 50\,\text{GeV}/c$, $\left|y^{\Upsilon}\right| < 1.2$. Therefore, the efficiencies are calculated under the assumption of unpolarised production of Υ mesons and no corresponding systematic uncertainty is assigned on the cross-section. Under the assumption of transversely polarised Υ mesons with $\lambda_\vartheta = 0.2$ in the LHCb kinematic region,[1] the total efficiency would result in an decrease of 3% [41].

5 Kinematic distributions of $\Upsilon\mathsf{C}$ events

The differential distributions are important for the determination of the production mechanism. In this section, the shapes of differential distributions for $\Upsilon(1\text{S})\text{D}^0$ and $\Upsilon(1\text{S})\text{D}^+$ events are studied. Assuming that the production mechanism of $\Upsilon\mathsf{C}$ events is essentially the same at $\sqrt{s} = 7$ and $8\,\text{TeV}$, both samples are treated together in this section.

The normalized differential distribution for each variable v is calculated as

$$\frac{1}{\sigma}\frac{\mathrm{d}\sigma}{\mathrm{d}v} = \frac{1}{N_{\text{corr}}^{\Upsilon\mathsf{C}}}\frac{N_{\text{corr},i}^{\Upsilon\mathsf{C}}}{\Delta v}, \tag{16}$$

where $N_{\text{corr},i}^{\Upsilon\mathsf{C}}$ is the number of efficiency-corrected signal events in bin i of width Δv, and $N_{\text{corr}}^{\Upsilon\mathsf{C}}$ is the total number of efficiency-corrected events. The differential distributions are presented for the following variables

- $p_{\text{T}}^{\Upsilon(1\text{S})}$, the transverse momentum of the $\Upsilon(1\text{S})$ meson;
- $p_{\text{T}}^{\mathsf{C}}$, the transverse momentum of the $\text{D}^0(\text{D}^+)$ meson;
- $y^{\Upsilon(1\text{S})}$, the rapidity of the $\Upsilon(1\text{S})$ meson;
- y^{C}, the rapidity of the $\text{D}^0(\text{D}^+)$ meson;
- $\Delta\phi = \phi^{\Upsilon(1\text{S})} - \phi^{\mathsf{C}}$, the difference in azimuthal angles between the $\Upsilon(1\text{S})$ and the C mesons;
- $\Delta y = y^{\Upsilon(1\text{S})} - y^{\mathsf{C}}$, the difference in rapidity between the $\Upsilon(1\text{S})$ and the C mesons;
- $p_{\text{T}}^{\Upsilon(1\text{S})\mathsf{C}}$, the transverse momentum of the $\Upsilon(1\text{S})\mathsf{C}$ system;

[1] The CMS measurements for $\Upsilon(1\text{S})$ mesons are consistent with small transverse polarisation in the helicity frame with the central values for the polarisation parameter $0 \lesssim \lambda_\vartheta \lesssim 0.2$ [70].

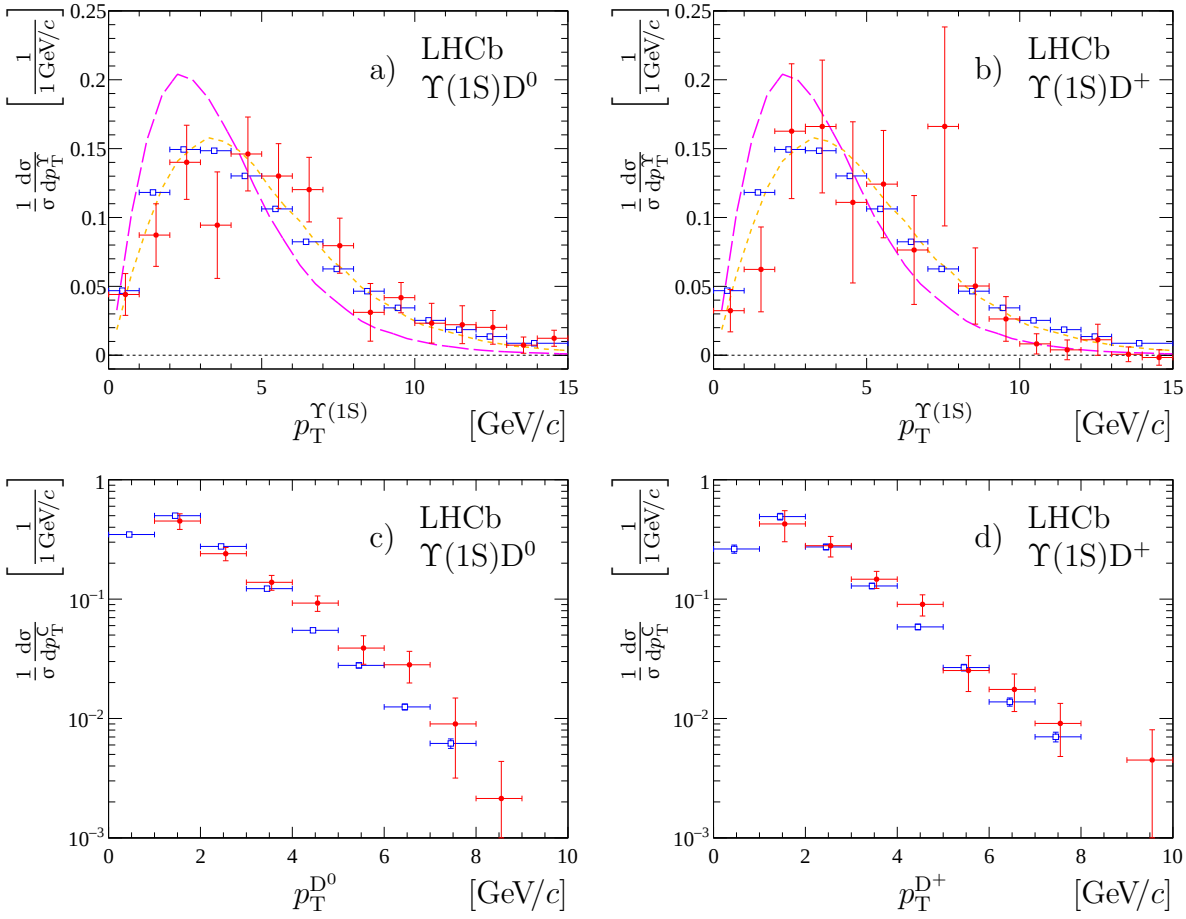

Figure 7: Background-subtracted and efficiency-corrected $p_{\rm T}^{\Upsilon}$ (top) and $p_{\rm T}^{\rm C}$ (bottom) distributions for $\Upsilon(1S)D^0$ events (left) and $\Upsilon(1S)D^+$ event (right). The transverse momentum spectra, derived within the DPS mechanism using the measurements from Refs. [38, 41], are shown with the open (blue) squares. The SPS predictions [72] for the $p_{\rm T}^{\Upsilon}$ spectra are shown with dashed (orange) and long-dashed (magenta) curves for calculations based on the $k_{\rm T}$-factorization and the collinear approximation, respectively. All distributions are normalized to unity.

- $y^{\Upsilon(1S)\rm C}$, the rapidity of the $\Upsilon(1S)\rm C$ system;
- $\mathscr{A}_{\rm T} = \dfrac{p_{\rm T}^{\Upsilon(1S)} - p_{\rm T}^{\rm C}}{p_{\rm T}^{\Upsilon(1S)} + p_{\rm T}^{\rm C}}$, the $p_{\rm T}$ asymmetry for the $\Upsilon(1S)$ and the $\rm C$ mesons;
- $m^{\Upsilon(1S)\rm C}$, the mass of the $\Upsilon(1S)\rm C$ system.

The distributions are shown in Figs. 7, 8, 9, 10 and 11. Only statistical uncertainties are displayed on these figures, as the systematic uncertainities discussed in Sect. 6 are small. For all variables the width of the resolution function is much smaller than the bin width, *i.e.* the results are not affected by bin-to-bin migration.

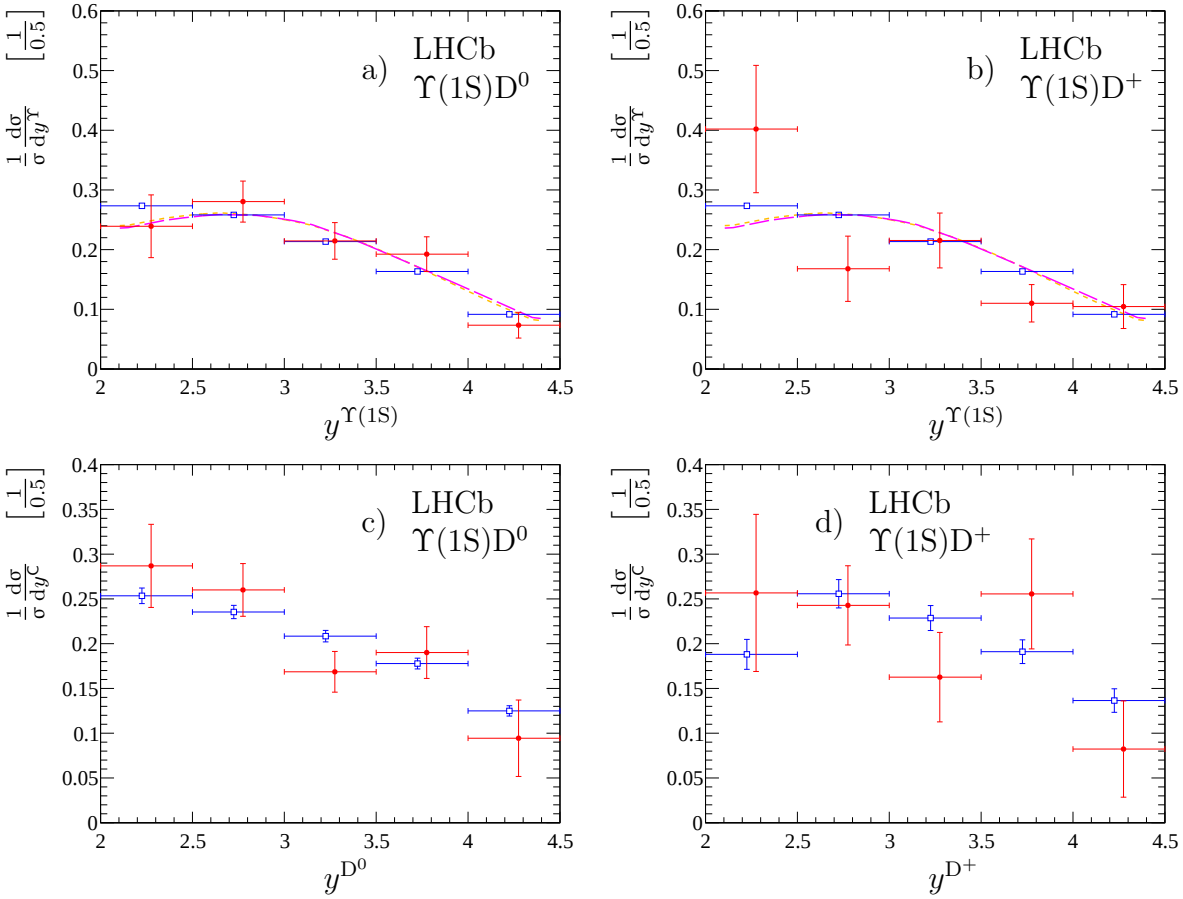

Figure 8: Background-subtracted and efficiency-corrected y^{Υ} (top) and y^{C} (bottom) distributions for $\Upsilon(1S)D^0$ (left) and $\Upsilon(1S)D^+$ (right) events. The rapidity spectra, derived within the DPS mechanism using the measurements from Refs. [38, 41], are shown with the open (blue) squares. The SPS predictions [72] for the y^{Υ} spectra are shown with dashed (orange) and long-dashed (magenta) curves for calculations based on the k_T-factorization and the collinear approximation, respectively. All distributions are normalized to unity.

The shapes of the measured differential distributions are compared with the SPS and DPS predictions. The DPS predictions are deduced from the measurements given in Refs. [38, 41], using a simplified simulation assuming uncorrelated production of the $\Upsilon(1S)$ and charm hadron. The agreement between all measured distributions and the DPS predictions is good. For the SPS mechanism, the predictions [72] based on k_T-factorization [17, 27–31] using the transverse momentum dependent gluon density from Refs. [32–34] are used along with the collinear approximation [26] with the leading-order gluon density taken from Ref. [73]. The transverse momentum and rapidity distributions of $\Upsilon(1S)$ mesons also agree well with SPS predictions based on k_T-factorization, while the shape of the transverse momentum spectra of Υ mesons disfavours the SPS predictions obtained using the collinear approximation. The shapes of the y^{Υ} distribution have very

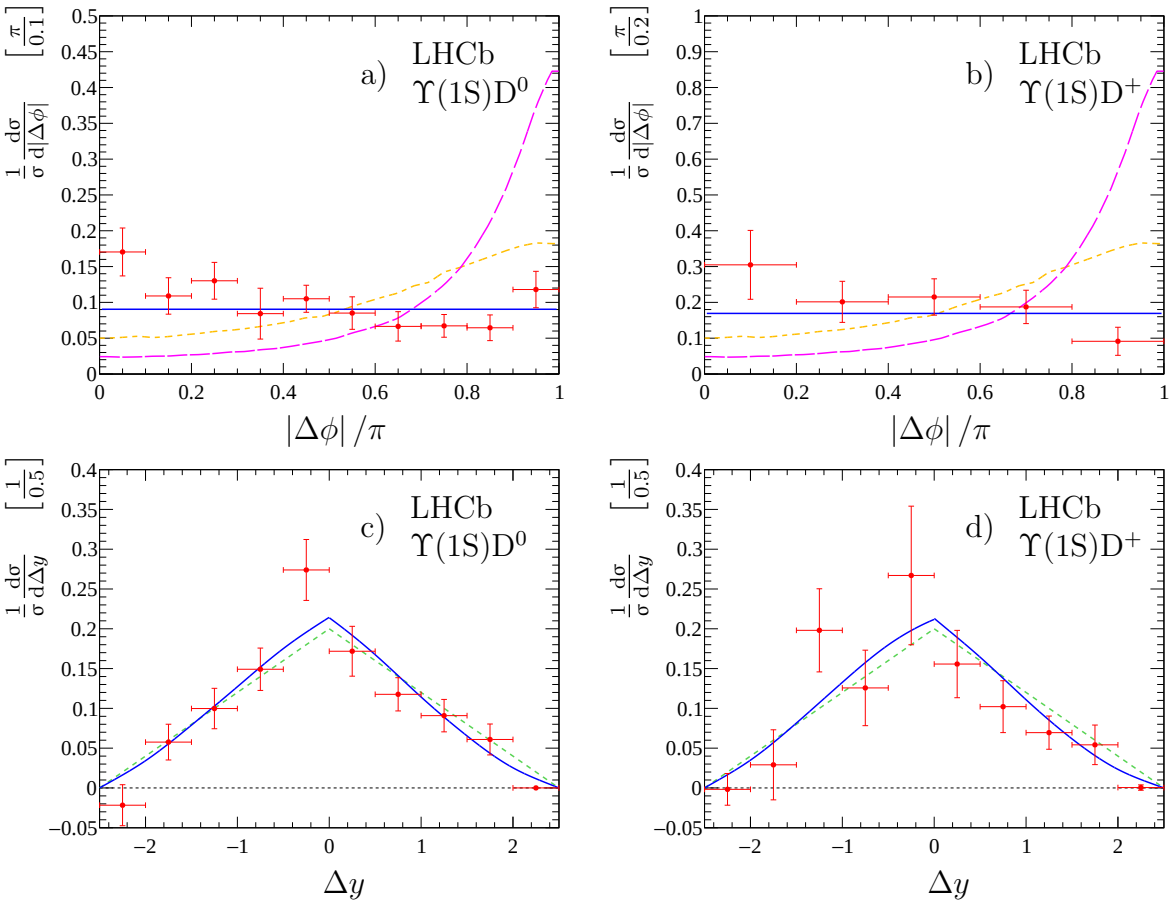

Figure 9: Background-subtracted and efficiency-corrected distributions for $|\Delta\phi|/\pi$ (top) and Δy (bottom) for $\Upsilon(1S)D^0$ (left) and $\Upsilon(1S)D^+$ (right) events. Straight lines in the $|\Delta\phi|/\pi$ plots show the result of the fit with a constant function. The SPS predictions [72] for the shapes of $\Delta\phi$ distribution are shown with dashed (orange) and long-dashed (magenta) curves for calculations based on the k_T-factorization and the collinear approximation, respectively. The solid (blue) curves in the Δy plots show the spectra obtained using a simplified simulation based on data from Refs. [38, 41]. The dashed (green) lines show the triangle function expected for totally uncorrelated production of two particles, uniformly distributed in rapidity. All distributions are normalized to unity.

limited sensitivity to the underlying production mechanism.

The distribution $|\Delta\phi|$ is presented in Fig. 9(a,b). The DPS mechanism predicts a flat distribution in $\Delta\phi$, while for SPS a prominent enhancement at $|\Delta\phi| \sim \pi$ is expected in collinear approximation. The enhancement is partly reduced taking into account transverse momenta of collinding partons [30, 74] and it is expected to be further smeared out at next-to-leading order. The measured distributions for $\Upsilon(1S)D^0$ and $\Upsilon(1S)D^+$ events, shown in Fig. 9(a,b) agree with a flat distribution. The fit result with a constant function gives a p-value of 6% (12%) for the $\Upsilon(1S)D^0$ ($\Upsilon(1S)D^+$) case, indicating that the SPS

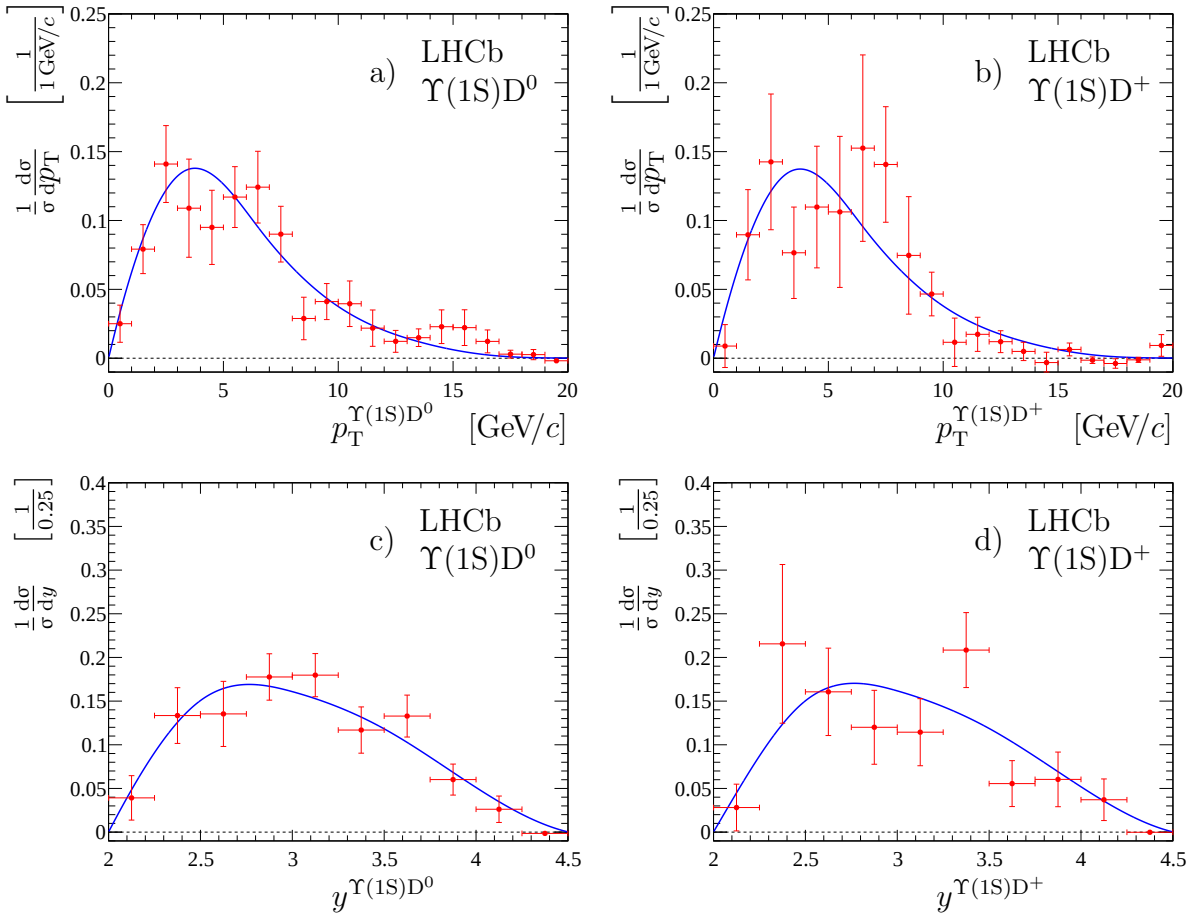

Figure 10: Background-subtracted and efficiency-corrected $p_T^{\Upsilon(1S)C}$ (top) and $y^{\Upsilon(1S)C}$ (bottom) distributions for $\Upsilon(1S)D^0$ (left) and $\Upsilon(1S)D^+$ (right) events. The blue curves show the spectra obtained using a simplified simulation based on data from Refs. [38, 41]. All distributions are normalized to unity.

contribution to the data is small. The shape of Δy distribution is defined primarily by the acceptance of LHCb experiment $2 < y < 4.5$ and has no sensitivity to the underlying production mechanism, in the limit of current statistics.

6 Systematic uncertainties

The systematic uncertainties related to the measurement of the production cross-section for ΥC pairs are summarized in Table 3 and discussed in detail in the following.

The signal shapes and parameters are taken from fits to large low-background inclusive $\Upsilon \to \mu^+\mu^-$ and charm samples. The parameters, signal peak positions and resolutions and the tail parameters for the double-sided Crystal Ball and the modified Novosibirsk functions, are varied within their uncertainties as determined from the calibration samples. The small

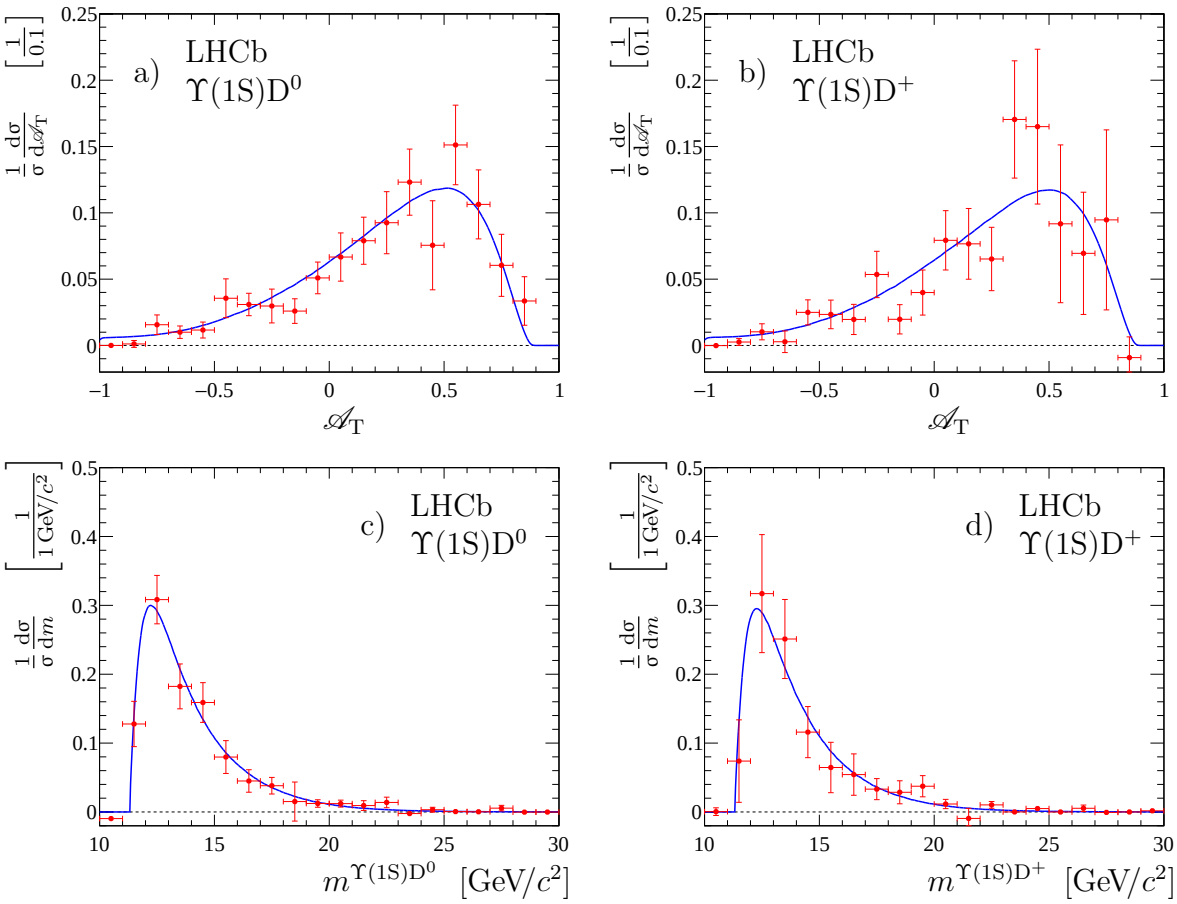

Figure 11: Background-subtracted and efficiency-corrected $\mathscr{A}_T$ (top) and $m^{\Upsilon(1S)C}$ (bottom) distributions for $\Upsilon(1S)D^0$ (left) and $\Upsilon(1S)D^+$ (right) events. The blue curves show the spectra obtained using a simplified simulation based on data from Refs. [38, 41]. All distributions are normalized to unity.

difference in parameters between the data sets obtained at $\sqrt{s} = 7$ and 8 TeV is also used to assign the systematic uncertainty. For D^0 and D^+ signal peaks alternative fit models have been used, namely a double-sided asymmetric variant of an Apolonious function [75] without power-law tail, a double-sided Crystal Ball function and an asymmetric Student-t shape. The systematic uncertainty related to the parameterization of the combinatorial background is determined by varying the order of the polynomial function in Eq. (7) between zeroth and second order. For the purely combinatorial background component (last line in Eq. (8)), a non-factorizable function is used

$$F^{BB}(m_{\mu^+\mu^-}, m_C) \propto e^{-\beta_1 m_{\mu^+\mu^-} - \beta_2 m_C} \times \left(\sum_{i=0}^{n} \sum_{j=0}^{k} \kappa_{ij}^2 P_n^i \left(m_{\mu^+\mu^-}\right) P_k^j \left(m_C\right) \right), \qquad (17)$$

where the parameters β_1, β_2 and $\kappa_{i,j}$ are allowed to float in the fit, and P_n^i and P_k^j are basic Bernstein polynomials, and the order of these polynomials, n and k, is varied between zero

Table 3: Summary of relative systematic uncertainties for $\sigma^{\Upsilon C}$ (in %). The total systematic uncertainty does not include the systematic uncertainty related to the knowledge of integrated luminosity [64]. The symbol $\oplus$ denotes the sum in quadrature.

Source	$\sigma^{\Upsilon D^0}$	$\sigma^{\Upsilon D^+}$
Signal ΥC extraction		
Υ and C signal shapes	$0.1 \oplus 0.3$	$0.1 \oplus 0.5$
2D fit model	0.4	0.7
Υ radiative tail	1.0	1.0
Efficiency corrections	0.1	1.3
Efficiency calculation		
muon identification	0.2	0.2
hadron identification	0.5	0.8
simulated samples size	0.2	0.2
tracking	$0.4 \oplus 4 \times 0.4$	$0.5 \oplus 5 \times 0.4$
hadronic interactions	2×1.4	3×1.4
trigger	2.0	2.0
data-simulation agreement	1.0	1.0
$\mathscr{B}_C$	1.3	2.1
Total	4.3	5.9

and two. The corresponding variations of ΥC signal yields are taken as the systematic uncertainty related to the description of the signal and background components.

Other systematic uncertainties are related to the imperfection of the PHOTOS generator [49] to describe the radiative tails in $\Upsilon \to \mu^+\mu^-$ decays. This systematic is studied in Ref. [76] and taken to be 1%.

The systematic uncertainty related to efficiency correction is estimated using an alternative technique for the determination of $N^{\Upsilon C}_{\rm corr}$, where the efficiency-corrected yields are obtained via

$$N^{\Upsilon C}_{\rm corr} = \sum_i \frac{w_i}{\varepsilon^{\rm tot}}, \tag{18}$$

where w_i is the signal event weight, obtained with the *sPlot* technique [63] using fits to the efficiency-uncorrected data sets, and $\varepsilon^{\rm tot}$ is a total efficiency for the given event, defined with Eq. (13). The difference in the efficiency-corrected yields with respect to the baseline approach of 0.1 (1.3)% for ΥD^0 (ΥD^+), is assigned as the corresponding systematic uncertainty.

The systematic uncertainty related to the particle identification is estimated to be 0.2% for muons and 0.5 (0.8)% for hadrons for the $\Upsilon(1S)D^0$ ($\Upsilon(1S)D^+$) case and is obtained from the uncertainties for the single particle identification efficiencies using an error propagation technique with a large number of pseudoexperiments. The same approach is

Table 4: Summary of relative systematic uncertainties for σ_{eff} (in %). The reduced uncertainty for C hadron production cross-section, denoted as $\delta(\sigma^{\mathsf{C}})$, is recalculated from Ref. [38] taking into account the cancellation of correlated systematic uncertainties.

Source	$\sigma_{\text{eff}}\vert_{\Upsilon \text{D}^0}$	$\sigma_{\text{eff}}\vert_{\Upsilon \text{D}^+}$
Signal $\Upsilon\mathsf{C}$ extraction		
Υ and C signal shapes	$0.1 \oplus 0.3$	$0.1 \oplus 0.5$
2D fit model	0.4	0.7
Efficiency corrections	0.1	1.3
Efficiency calculation		
hadron identification	0.5	0.8
simulated samples size	0.2	0.2
$\delta(\sigma^{\mathsf{C}})$	6.7	9.7
FONLL extrapolation ($\sqrt{s} = 8\,\text{TeV}$ only)	2.1	2.1
Total $\sqrt{s} = 7\,\text{TeV}$	6.7	9.9
Total $\sqrt{s} = 8\,\text{TeV}$	7.0	10.1

Table 5: Summary of relative systematic uncertainties for the ratios $R^{\Upsilon\mathsf{C}}$ and $R^{\text{D}^0/\text{D}^+}$ (in %).

Source	$R^{\Upsilon \text{D}^0}$	$R^{\Upsilon \text{D}^+}$	$R^{\text{D}^0/\text{D}^+}$
Signal extraction			
Υ and C signal shapes	$0.1 \oplus 0.3$	$0.1 \oplus 0.5$	$0.3 \oplus 0.5$
2D fit model	0.4	0.7	$0.4 \oplus 0.7$
Efficiency corrections	0.1	1.3	$0.1 \oplus 1.3$
Efficiency calculation:			
hadron identification	0.5	0.8	$0.5 \oplus 0.8$
tracking	$0.4 \oplus 4 \times 0.4$	$0.5 \oplus 5 \times 0.4$	$0.6 \oplus 1 \times 0.4$
hadronic interactions	2×1.4	3×1.4	1×1.4
data-simulation agreement	1.0	1.0	$1.0 \oplus 1.0$
simulated samples size	0.2	0.2	$0.2 \oplus 0.2$
$\mathscr{B}_{\mathsf{C}}$	1.3	2.1	$1.3 \oplus 2.1$
Total	3.4	5.3	3.8

used to propagate the uncertainties in ε^{acc}, ε^{rec} and ε^{trg} related to the limited simulation sample size.

The efficiency is corrected using data-driven techniques to account for small differences in the tracking efficiency between data and simulation [54, 55]. The uncertainty in the correction factor is propagated to the cross-section measurement using pseudoexperiments

resulting in a global 0.4 (0.5)% systematic uncertainty for the ΥD^0 (ΥD^+) cases plus an additional uncertainty of 0.4% per track. The knowledge of the hadronic interaction length of the detector results in an uncertainty of 1.4% per final-state hadron [54].

The systematic uncertainty associated with the trigger requirements is assessed by studying the performance of the dimuon trigger for $\Upsilon(1S)$ events selected using the single muon high-p_T trigger [45] in data and simulation. The comparison is performed in bins of the $\Upsilon(1S)$ meson transverse momentum and rapidity and the largest observed difference of 2.0% is assigned as the systematic uncertainty associated with the imperfection of trigger simulation [41].

Using large samples of low-background inclusive $\Upsilon \to \mu^+\mu^-$, $D^0 \to K^-\pi^+$ and $D^+ \to K^-\pi^+\pi^+$ events, good agreement between data and simulation is observed for the selection variables used in this analysis, in particular for dimuon and charm vertex quality and $\chi^2_{\rm fit}(\Upsilon)/{\rm ndf}$. The small differences seen would affect the efficiencies by less than 1.0%, which is conservatively taken as a systematic uncertainty accounting for the disagreement between data and simulation.

The systematic uncertainty related to the uncertainties of the branching fractions of D^0 and D^+ mesons is 1.3% and 2.1% [42]. The integrated luminosity is measured using a beam-gas imaging method [77, 78]. The absolute luminosity scale is determined with 1.7 (1.2)% uncertainty for the sample collected at $\sqrt{s} = 7\,(8)$ TeV, dominated by the vertex resolution for beam-gas interactions, the spread of the measurements and the detector alignment [64, 78, 79].

The selection criteria favour the selection of charm hadrons produced promptly at the pp collision vertex and significantly suppress the feed down from charm hadrons produced in decays of beauty hadrons. The remaining feed down is estimated separately for DPS and SPS processes with the simultaneous production of an Υ meson and a $b\overline{b}$-pair. The former is estimated using simulation, normalized to the measured $b\overline{b}$ and $c\overline{c}$ production cross-sections [38, 80] and validated using a data-driven technique. It is found to be smaller than 1.5% of the observed signal and is neglected. The contribution from SPS processes with the associated production of Υ meson and $b\overline{b}$ pairs is estimated using the prediction for the ratio of production cross-sections,

$$\frac{\sigma^{\Upsilon b\overline{b}}}{\sigma^{\Upsilon c\overline{c}}} = (2-5)\%\,, \tag{19}$$

obtained using the k_T-factorization approach with the transverse momentum dependent gluon density taken from Refs. [32–34]. The uncertainty reflects the variation of scale and the difference with results obtained using the collinear approximation with the gluon density from Ref. [73]. Combining the estimates from Eqs. (19), (1) and (2) with the probability for a charm hadron from the decay of beauty hadron to pass the selection criteria, this feed down is found to be totally negligible.

The effect of possible extreme polarization scenarios for Υ mesons from SPS processes is proportional to the SPS contamination, $\alpha_{\rm SPS}$, and could lead to $+0.08\,(-0.16)\alpha_{\rm SPS}$ correction [68] to the cross-sections $\sigma^{\Upsilon C}$ and the ratios $R^{\Upsilon C}$ for totally transverse (longitudinal) polarizations of Υ mesons in centre-of-mass helicity frame. It is very small for small

SPS contamination. The corresponding corrections to ratios $R^{\mathrm{D^0/D^+}}$ are non-zero only if SPS has different contributions to $\Upsilon\mathrm{D}^0$ and $\Upsilon\mathrm{D}^+$ production processes and accouts for $+0.08\,(-0.16)\Delta\alpha_{\mathrm{SPS}}$, where $\Delta\alpha_{\mathrm{SPS}}$ is the difference in SPS contaminations to the considered processes. The same estimate is valid also for the ratios $R^{\Upsilon(1\mathrm{S})/\Upsilon(2\mathrm{S})}$.

A large part of the systematic uncertainties cancels in the ratio $R^{\Upsilon\mathsf{C}}$ and in the variable σ_{eff}. The systematic uncertainties for σ_{eff}, $R^{\Upsilon\mathsf{C}}$ and $R^{\mathrm{D^0/D^+}}$ are summarized in Tables 4 and 5. For the production cross-section of charm mesons at $\sqrt{s} = 8\,\mathrm{TeV}$ the measured cross-section at $\sqrt{s} = 7\,\mathrm{TeV}$ is extrapolated using FONLL calculations [65–67]. The uncertainty related to the imperfection of the extrapolation is estimated from the comparison of the measured ratio $\sigma^{\mathsf{C}}_{\sqrt{s}=13\,\mathrm{TeV}}/\sigma^{\mathsf{C}}_{\sqrt{s}=7\,\mathrm{TeV}}$ [38, 81] and the corresponding FONLL estimate. As a result of this comparison the C hadron production cross-section is scaled up by 2.7% and a systematic uncertainty of 2.1% is assigned. The systematic uncertainty for the ratios $R^{\Upsilon(2\mathrm{S})/\Upsilon(1\mathrm{S})}_{\mathsf{C}}$ is small compared to the statistical uncertainty and is neglected.

7 Results and discussion

The associated production of Υ and charm mesons is studied. Pair production of $\Upsilon(1\mathrm{S})\mathrm{D}^0$, $\Upsilon(2\mathrm{S})\mathrm{D}^0$, $\Upsilon(1\mathrm{S})\mathrm{D}^+$, $\Upsilon(2\mathrm{S})\mathrm{D}^+$ and $\Upsilon(1\mathrm{S})\mathrm{D}_{\mathrm{s}}^+$ states is observed with significances exceeding five standard deviations. The production cross-sections in the fiducial region $2.0 < y^{\Upsilon} < 4.5$, $p_{\mathrm{T}}^{\Upsilon} < 15\,\mathrm{GeV}/c$, $2.0 < y^{\mathsf{C}} < 4.5$ and $1 < p_{\mathrm{T}}^{\mathsf{C}} < 20\,\mathrm{GeV}/c$ are measured for $\Upsilon(1\mathrm{S})\mathrm{D}^0$ and $\Upsilon(1\mathrm{S})\mathrm{D}^+$ final states at $\sqrt{s} = 7$ and $8\,\mathrm{TeV}$ as:

$$
\begin{aligned}
\mathscr{B}_{\mu^+\mu^-} \times \sigma^{\Upsilon(1\mathrm{S})\mathrm{D}^0}_{\sqrt{s}=7\,\mathrm{TeV}} &= 155 \pm 21\,(\mathrm{stat}) \pm 7\,(\mathrm{syst})\,\mathrm{pb}\,,\\
\mathscr{B}_{\mu^+\mu^-} \times \sigma^{\Upsilon(1\mathrm{S})\mathrm{D}^+}_{\sqrt{s}=7\,\mathrm{TeV}} &= 82 \pm 19\,(\mathrm{stat}) \pm 5\,(\mathrm{syst})\,\mathrm{pb}\,,\\
\mathscr{B}_{\mu^+\mu^-} \times \sigma^{\Upsilon(1\mathrm{S})\mathrm{D}^0}_{\sqrt{s}=8\,\mathrm{TeV}} &= 250 \pm 28\,(\mathrm{stat}) \pm 11\,(\mathrm{syst})\,\mathrm{pb}\,,\\
\mathscr{B}_{\mu^+\mu^-} \times \sigma^{\Upsilon(1\mathrm{S})\mathrm{D}^+}_{\sqrt{s}=8\,\mathrm{TeV}} &= 80 \pm 16\,(\mathrm{stat}) \pm 5\,(\mathrm{syst})\,\mathrm{pb}\,,
\end{aligned}
$$

where the first uncertainty is statistical, and the second is the systematic uncertainty from Table 3, combined with the uncertainty related to the knowledge of the luminosity. All these measurements are statistically limited. The measured cross-sections are in agreement with the DPS expectations from Eq. (5), and significantly exceed the expectations from the SPS mechanism in Eqs. (1) and (2). Differential kinematic distributions are studied for $\Upsilon\mathrm{D}^0$ and $\Upsilon\mathrm{D}^+$ final states. All of them are in good agreement with DPS expectations as the main production mechanism.

The ratios of the cross-sections for $\Upsilon(1S)D^0$ and $\Upsilon(1S)D^+$ are

$$R^{D^0/D^+}_{\sqrt{s}=7\,\text{TeV}} = \frac{\sigma^{\Upsilon(1S)D^0}_{\sqrt{s}=7\,\text{TeV}}}{\sigma^{\Upsilon(1S)D^+}_{\sqrt{s}=7\,\text{TeV}}} = 1.9 \pm 0.5\,(\text{stat}) \pm 0.1\,(\text{syst})\,,$$

$$R^{D^0/D^+}_{\sqrt{s}=8\,\text{TeV}} = \frac{\sigma^{\Upsilon(1S)D^0}_{\sqrt{s}=8\,\text{TeV}}}{\sigma^{\Upsilon(1S)D^+}_{\sqrt{s}=8\,\text{TeV}}} = 3.1 \pm 0.7\,(\text{stat}) \pm 0.1\,(\text{syst})\,,$$

where the systematic uncertainty is discussed in detail in Sect. 6. The results are compatible with the DPS expectation of 2.41 ± 0.18 from Eq. (6a).

The cross-section ratios $R^{\Upsilon C}$ are measured to be

$$R^{\Upsilon(1S)D^0}_{\sqrt{s}=7\,\text{TeV}} = \left.\frac{\sigma^{\Upsilon(1S)D^0}}{\sigma^{\Upsilon(1S)}}\right|_{\sqrt{s}=7\,\text{TeV}} = (6.3 \pm 0.8\,(\text{stat}) \pm 0.2\,(\text{syst}))\,\%\,,$$

$$R^{\Upsilon(1S)D^+}_{\sqrt{s}=7\,\text{TeV}} = \left.\frac{\sigma^{\Upsilon(1S)D^+}}{\sigma^{\Upsilon(1S)}}\right|_{\sqrt{s}=7\,\text{TeV}} = (3.4 \pm 0.8\,(\text{stat}) \pm 0.2\,(\text{syst}))\,\%\,,$$

$$R^{\Upsilon(1S)D^0}_{\sqrt{s}=8\,\text{TeV}} = \left.\frac{\sigma^{\Upsilon(1S)D^0}}{\sigma^{\Upsilon(1S)}}\right|_{\sqrt{s}=8\,\text{TeV}} = (7.8 \pm 0.9\,(\text{stat}) \pm 0.3\,(\text{syst}))\,\%\,,$$

$$R^{\Upsilon(1S)D^+}_{\sqrt{s}=8\,\text{TeV}} = \left.\frac{\sigma^{\Upsilon(1S)D^+}}{\sigma^{\Upsilon(1S)}}\right|_{\sqrt{s}=8\,\text{TeV}} = (2.5 \pm 0.5\,(\text{stat}) \pm 0.1\,(\text{syst}))\,\%\,.$$

Extrapolating the ratios $R^{\Upsilon C}$ down to $p_{\text{T}}^{C} = 0$ using the measured transverse momentum spectra of D^0 and D^+ mesons from Ref. [38], and using the fragmentation fractions $f(c \to D^0) = 0.565 \pm 0.032$ and $f(c \to D^+) = 0.246 \pm 0.020$, measured at e^+e^- colliders operating at a centre-of-mass energy close to the $\Upsilon(4S)$ resonance [82], the ratios $R^{\Upsilon c\bar{c}}$ are calculated to be

$$R^{\Upsilon(1S)c\bar{c}}_{\sqrt{s}=7\,\text{TeV}} = \left.\frac{\sigma^{\Upsilon(1S)c\bar{c}}}{\sigma^{\Upsilon(1S)}}\right|_{\sqrt{s}=7\,\text{TeV}} = (7.7 \pm 1.0)\,\%\,,$$

$$R^{\Upsilon(1S)c\bar{c}}_{\sqrt{s}=8\,\text{TeV}} = \left.\frac{\sigma^{\Upsilon(1S)c\bar{c}}}{\sigma^{\Upsilon(1S)}}\right|_{\sqrt{s}=8\,\text{TeV}} = (8.0 \pm 0.9)\,\%\,,$$

which significantly exceed SPS expectations from Eqs. (1) and (2).

The large statistical uncertainty for the other ΥC modes does not allow to obtain a numerical model-independent measurement, but, assuming similar kinematics for $\Upsilon(2S)$ and charm mesons to the prompt production, the following ratios are measured

$$R^{\Upsilon(2S)/\Upsilon(1S)}_{D^0} = \mathscr{B}_{2/1} \times \frac{\sigma^{\Upsilon(2S)D^0}_{\sqrt{s}=7\,\text{TeV}}}{\sigma^{\Upsilon(1S)D^0}_{\sqrt{s}=7\,\text{TeV}}} = (13 \pm 5)\%\,,$$

$$R^{\Upsilon(2S)/\Upsilon(1S)}_{D^0} = \mathscr{B}_{2/1} \times \frac{\sigma^{\Upsilon(2S)D^0}_{\sqrt{s}=8\,\text{TeV}}}{\sigma^{\Upsilon(1S)D^0}_{\sqrt{s}=8\,\text{TeV}}} = (20 \pm 4)\%\,,$$

where $\mathscr{B}_{2/1}$ is the ratio of dimuon branching fractions of $\Upsilon(2S)$ and $\Upsilon(1S)$ mesons and where the systematic uncertainties are negligible compared to statistical uncertainties. These values are smaller than, but compatible with the DPS expectations from Eq. (6b). For the ΥD^+ production one obtains

$$R_{D^+}^{\Upsilon(2S)/\Upsilon(1S)} = \mathscr{B}_{2/1} \times \frac{\sigma^{\Upsilon(2S)D^+}_{\sqrt{s}=7\,\mathrm{TeV}}}{\sigma^{\Upsilon(1S)D^+}_{\sqrt{s}=7\,\mathrm{TeV}}} = (22 \pm 7)\%\,,$$

$$R_{D^+}^{\Upsilon(2S)/\Upsilon(1S)} = \mathscr{B}_{2/1} \times \frac{\sigma^{\Upsilon(2S)D^+}_{\sqrt{s}=8\,\mathrm{TeV}}}{\sigma^{\Upsilon(1S)D^+}_{\sqrt{s}=8\,\mathrm{TeV}}} = (22 \pm 6)\%\,,$$

where again the systematic uncertainties are negligible with respect to the statistical ones and are ignored. These values are compatible with the DPS expectation of 25% from Eq. (6b).

Neglecting the contributions from SPS mechanism, the effective cross-section σ_{eff} is determined using Eq. (10a) for the $\sqrt{s} = 7\,\mathrm{TeV}$ data as

$$\begin{aligned}\sigma_{\mathrm{eff}}|_{\Upsilon(1S)D^0} &= 19.4 \pm 2.6\,(\mathrm{stat}) \pm 1.3\,(\mathrm{syst})\,\mathrm{mb}\,,\\ \sigma_{\mathrm{eff}}|_{\Upsilon(1S)D^+} &= 15.2 \pm 3.6\,(\mathrm{stat}) \pm 1.5\,(\mathrm{syst})\,\mathrm{mb}\,.\end{aligned}$$

The central values of σ_{eff} increase by up to 10% if SPS contribution exceeds by a factor of two the central value from Eq. (1). Both values are consistent with previous measurements of σ_{eff} [11, 15, 40, 83–88], and their average is

$$\sigma_{\mathrm{eff}}|_{\Upsilon(1S)D^{0,+},\sqrt{s}=7\,\mathrm{TeV}} = 18.0 \pm 2.1\,(\mathrm{stat}) \pm 1.2\,(\mathrm{syst}) = 18.0 \pm 2.4\,\mathrm{mb}\,.$$

For the $\sqrt{s} = 8\,\mathrm{TeV}$ data the effective cross-section σ_{eff} is estimated using the measured $\Upsilon(1S)$ cross-section at $\sqrt{s} = 8\,\mathrm{TeV}$ [41] combined with σ^{c}, extrapolated from $\sqrt{s} = 7\,\mathrm{TeV}$ [38] to $\sqrt{s} = 8\,\mathrm{TeV}$ using FONLL calculations [65–67]. The obtained effective DPS cross-sections are:

$$\begin{aligned}\sigma_{\mathrm{eff}}|_{\Upsilon(1S)D^0} &= 17.2 \pm 1.9\,(\mathrm{stat}) \pm 1.2\,(\mathrm{syst})\,\mathrm{mb}\,,\\ \sigma_{\mathrm{eff}}|_{\Upsilon(1S)D^+} &= 22.3 \pm 4.4\,(\mathrm{stat}) \pm 2.2\,(\mathrm{syst})\,\mathrm{mb}\,,\end{aligned}$$

The mean value of

$$\sigma_{\mathrm{eff}}|_{\Upsilon(1S)D^{0,+},\sqrt{s}=8\,\mathrm{TeV}} = 17.9 \pm 1.8\,(\mathrm{stat}) \pm 1.2\,(\mathrm{syst}) = 17.9 \pm 2.1\,\mathrm{mb}\,, \qquad (20)$$

is in good agreement with those obtained for $\sqrt{s} = 7\,\mathrm{TeV}$ data. Averaging these values, σ_{eff} is found to be

$$\sigma_{\mathrm{eff}}|_{\Upsilon(1S)D^{0,+}} = 18.0 \pm 1.3\,(\mathrm{stat}) \pm 1.2\,(\mathrm{syst}) = 18.0 \pm 1.8\,\mathrm{mb}\,.$$

The large value of the cross-section for the associated production of Υ and open charm hadrons, compatible with the DPS estimate of Eq. (4), has important consequences for the interpretation of heavy-flavor production measurements, especially inclusive measurements and possibly for b-flavor tagging [89–92], where the production of uncorrelated charm hadrons could affect the right assignment of the initial flavour of the studied beauty hadron.

8 Summary

The associated production of Υ mesons with open charm hadrons is observed in pp collisions at centre-of-mass energies of 7 and 8 TeV using data samples corresponding to integrated luminosities of $1\,\text{fb}^{-1}$ and $2\,\text{fb}^{-1}$ respectively, collected with the LHCb detector. The production of $\Upsilon(1S)D^0$, $\Upsilon(2S)D^0$, $\Upsilon(1S)D^+$, $\Upsilon(2S)D^+$ and $\Upsilon(1S)D_s^+$ pairs is observed with significances larger than 5 standard deviations. The production cross-sections in the fiducial region $2.0 < y^{\Upsilon} < 4.5$, $p_{\rm T}^{\Upsilon} < 15\,\text{GeV}/c$, $2.0 < y^{\rm C} < 4.5$ and $1 < p_{\rm T}^{\rm C} < 20\,\text{GeV}/c$ are measured for $\Upsilon(1S)D^0$ and $\Upsilon(1S)D^+$ final states at $\sqrt{s} = 7$ and 8 TeV. The measured cross-sections are in agreement with DPS expectations and significantly exceed the expectations from the SPS mechanism. The differential kinematic distributions for ΥD^0 and ΥD^+ are studied and all are found to be in good agreement with the DPS expectations as the main production mechanism. The measured effective cross-section $\sigma_{\rm eff}$ is in agreement with most previous measurements.

Acknowledgements

We thank J. R. Gaunt, P. Gunnellini, M. Diehl, A. K. Likhoded, A. V. Luchinsky, R. Maciuła, S. Poslavsky and A. Szczurek for interesting and stimulating discussions on the SPS and DPS mechanisms. We are greatly indebted to S. P. Baranov for providing us with predictions Eqs. (2) and (19) and the differential kinematic distributions for $\Upsilon + c\bar{c}$ SPS process. We express our gratitude to our colleagues in the CERN accelerator departments for the excellent performance of the LHC. We thank the technical and administrative staff at the LHCb institutes. We acknowledge support from CERN and from the national agencies: CAPES, CNPq, FAPERJ and FINEP (Brazil); NSFC (China); CNRS/IN2P3 (France); BMBF, DFG and MPG (Germany); INFN (Italy); FOM and NWO (The Netherlands); MNiSW and NCN (Poland); MEN/IFA (Romania); MinES and FANO (Russia); MinECo (Spain); SNSF and SER (Switzerland); NASU (Ukraine); STFC (United Kingdom); NSF (USA). We acknowledge the computing resources that are provided by CERN, IN2P3 (France), KIT and DESY (Germany), INFN (Italy), SURF (The Netherlands), PIC (Spain), GridPP (United Kingdom), RRCKI (Russia), CSCS (Switzerland), IFIN-HH (Romania), CBPF (Brazil), PL-GRID (Poland) and OSC (USA). We are indebted to the communities behind the multiple open source software packages on which we depend. We are also thankful for the computing resources and the access to software R&D tools provided by Yandex LLC (Russia). Individual groups or members have received support from AvH Foundation (Germany), EPLANET, Marie Skłodowska-Curie Actions and ERC (European Union), Conseil Général de Haute-Savoie, Labex ENIGMASS and OCEVU, Région Auvergne (France), RFBR (Russia), GVA, XuntaGal and GENCAT (Spain), The Royal Society and Royal Commission for the Exhibition of 1851 (United Kingdom).

References

[1] NA3 collaboration, J. Badier *et al.*, *Evidence for* $\psi\psi$ *production in* π^- *interactions at* 150 GeV/c *and* 280 GeV/c, Phys. Lett. **B114** (1982) 457.

[2] NA3 collaboration, J. Badier *et al.*, $\psi\psi$ *production and limits on beauty meson production from* 400 GeV/c *protons*, Phys. Lett. **B158** (1985) 85.

[3] WA75 collaboration, S. Aoki *et al.*, *The double associated production of charmed particles by the interaction of* 350 GeV/c π^- *mesons with emulsion nuclei*, Phys. Lett. **B187** (1987) 185.

[4] LHCb collaboration, R. Aaij *et al.*, *Observation of* J/ψ *-pair production in* pp *collisions at* $\sqrt{s} = 7$ TeV, Phys. Lett. **B707** (2012) 52, arXiv:1109.0963.

[5] A. V. Berezhnoy, A. K. Likhoded, A. V. Luchinsky, and A. A. Novoselov, *Double* J/ψ *-meson production at LHC and 4*c*-tetraquark state*, Phys. Rev. **D84** (2011) 094023, arXiv:1101.5881.

[6] S. P. Baranov, *Pair production of* J/ψ *mesons in the* $k_{\rm T}$*-factorization approach*, Phys. Rev. **D84** (2011) 054012.

[7] C. H. Kom, A. Kulesza, and W. J. Stirling, *Pair production of* J/ψ *as a probe of double parton scattering at LHCb*, Phys. Rev. Lett. **107** (2011) 082002, arXiv:1105.4186.

[8] N. Paver and D. Treleani, *Multi-quark scattering and large* $p_{\rm T}$ *jet production in hadronic hollisions*, Nuovo Cim. **A70** (1982) 215.

[9] M. Diehl and A. Schafer, *Theoretical considerations on multiparton interactions in QCD*, Phys. Lett. **B698** (2011) 389, arXiv:1102.3081.

[10] M. Diehl, D. Ostermeier, and A. Schafer, *Elements of a theory for multiparton interactions in QCD*, JHEP **03** (2012) 089, arXiv:1111.0910.

[11] S. Bansal *et al.*, *Progress in double parton scattering studies*, arXiv:1410.6664.

[12] A. Szczurek, *A short review of some double-parton scattering processes*, Acta Phys. Polon. Supp. **8** (2015), no. 2 483, arXiv:1505.04067.

[13] D0 collaboration, V. M. Abazov *et al.*, *Observation and studies of double* J/ψ *production at the Tevatron*, Phys. Rev. **D90** (2014) 111101, arXiv:1406.2380.

[14] CMS collaboration, V. Khachatryan *et al.*, *Measurement of prompt* J/ψ *pair production in* pp *collisions at* $\sqrt{s} = 7$ TeV, JHEP **09** (2014) 094, arXiv:1406.0484.

[15] LHCb collaboration, R. Aaij *et al.*, *Observation of double charm production involving open charm in* pp *collisions at* $\sqrt{s} = 7$ TeV, JHEP **06** (2012) 141, Addendum ibid. **03** (2014) 108, arXiv:1205.0975.

[16] A. V. Berezhnoy, V. V. Kiselev, A. K. Likhoded, and A. I. Onishchenko, *Doubly charmed baryon production in hadronic experiments*, Phys. Rev. **D57** (1998) 4385, arXiv:hep-ph/9710339.

[17] S. P. Baranov, *Topics in associated* $\mathrm{J/\psi} + \mathrm{c} + \bar{\mathrm{c}}$ *production at modern colliders*, Phys. Rev. **D73** (2006) 074021.

[18] J.-P. Lansberg, *On the mechanisms of heavy-quarkonium hadroproduction*, Eur. Phys. J. **C61** (2009) 693, arXiv:0811.4005.

[19] R. Maciuła, A. van Hameren, and A. Szczurek, *Charm meson production and double parton interactions at the LHC*, Acta Phys. Polon. **B45** (2014), no. 7 1493, arXiv:1404.0891.

[20] R. Maciuła and A. Szczurek, *Single and double charmed meson production at the LHC*, EPJ Web Conf. **81** (2014) 01007.

[21] CDF collaboration, F. Abe *et al.*, *Observation of the* $\mathrm{B_c^+}$ *meson in* $\mathrm{p\overline{p}}$ *collisions at* $\sqrt{s} = 1.8\,\mathrm{TeV}$, Phys. Rev. Lett. **81** (1998) 2432, arXiv:hep-ex/9805034.

[22] LHCb collaboration, R. Aaij *et al.*, *Measurement of* $\mathrm{B_c^+}$ *production at* $\sqrt{s} = 8\,\mathrm{TeV}$, Phys. Rev. Lett. **114** (2014) 132001, arXiv:1411.2943.

[23] A. V. Berezhnoy, A. K. Likhoded, and M. V. Shevlyagin, *Hadronic production of* $\mathrm{B_c^+}$ *mesons*, Phys. Atom. Nucl. **58** (1995) 672, arXiv:hep-ph/9408284.

[24] K. Kołodziej, A. Leike, and R. Rückl, *Production of* $\mathrm{B_c^+}$ *mesons in hadronic collisions*, Phys. Lett. **B355** (1995) 337, arXiv:hep-ph/9505298.

[25] C.-H. Chang, Y.-Q. Chen, G.-P. Han, and H.-T. Jiang, *On hadronic production of the* $\mathrm{B_c^+}$ *meson*, Phys. Lett. **B364** (1995) 78, arXiv:hep-ph/9408242.

[26] A. V. Berezhnoy and A. K. Likhoded, *Associated production of* Υ *and open charm at LHC*, Int. J. Mod. Phys. **A30** (2015) 1550125, arXiv:1503.04445.

[27] L. V. Gribov, E. M. Levin, and M. G. Ryskin, *Semihard Processes in QCD*, Phys. Rept. **100** (1983) 1; E. M. Levin and M. G. Ryskin, *High-energy hadron collisions in QCD*, Phys. Rept. **189** (1990) 267.

[28] S. P. Baranov, *Highlights from the* k_{T} *factorization approach on the quarkonium production puzzles*, Phys. Rev. **D66** (2002) 114003, [,162(2002)].

[29] Small x collaboration, B. Andersson *et al.*, *Small-x phenomenology: Summary and status*, Eur. Phys. J. **C25** (2002) 77, arXiv:hep-ph/0204115; J. R. Andersen *et al.*, *Small-x phenomenology: Summary and status*, Eur. Phys. J. **C35** (2004) 67, arXiv:hep-ph/0312333; J. R. Andersen *et al.*, *Small-x phenomenology: Summary of the 3rd Lund Small-x Workshop in 2004*, Eur. Phys. J. **C48** (2006) 53, arXiv:hep-ph/0604189.

[30] S. P. Baranov, *Associated* Υ + b + $\overline{\text{b}}$ *production at the Fermilab Tevatron and CERN LHC*, Phys. Rev. **D74** (2006) 074002.

[31] S. P. Baranov, *Prompt* Υ(nS) *production at the LHC in view of the* k_{T} *-factorization approach*, Phys. Rev. **D86** (2012) 054015.

[32] H. Jung and F. Hautmann, *Determination of transverse momentum dependent gluon density from HERA structure function measurements*, in *Proceedings, 20th International Workshop on Deep-Inelastic Scattering and Related Subjects (DIS 2012)*, pp. 433–436, 2012. arXiv:1206.1796. [,433(2012)], doi: 10.3204/DESY-PROC-2012-02/29.

[33] F. Hautmann and H. Jung, *Transverse momentum dependent gluon density from DIS precision data*, Nucl. Phys. **B883** (2014) 1, arXiv:1312.7875.

[34] H. Jung and F. Hautmann, *Transverse momentum dependent gluon density from DIS precision data*, PoS **DIS2014** (2014) 042.

[35] G. Calucci and D. Treleani, *Minijets and the two-body parton correlation*, Phys. Rev. **D57** (1998) 503, arXiv:hep-ph/9707389.

[36] G. Calucci and D. Treleani, *Proton structure in transverse space and the effective cross section*, Phys. Rev. **D60** (1999) 054023, arXiv:hep-ph/9902479.

[37] A. Del Fabbro and D. Treleani, *Scale factor in double parton collisions and parton densities in transverse space*, Phys. Rev. **D63** (2001) 057901, arXiv:hep-ph/0005273.

[38] LHCb collaboration, R. Aaij *et al.*, *Prompt charm production in* pp *collisions at* $\sqrt{s} = 7\,\text{TeV}$, Nucl. Phys. **B871** (2013) 1, arXiv:1302.2864.

[39] CDF collaboration, F. Abe *et al.*, *Measurement of double parton scattering in* $\overline{\text{p}}$p *collisions at* $\sqrt{s} = 1.8\,\text{TeV}$, Phys. Rev. Lett. **79** (1997) 584.

[40] CDF collaboration, F. Abe *et al.*, *Double parton scattering in* $\overline{\text{p}}$p *collisions at* $\sqrt{s} = 1.8\,\text{TeV}$, Phys. Rev. **D56** (1997) 3811.

[41] R. Aaij *et al.*, *Forward production of* Υ *mesons in* pp *collisions at* $\sqrt{s} = 7$ *and* $8\,\text{TeV}$, JHEP **11** (2015) 103, arXiv:1509.02372.

[42] Particle Data Group, K. A. Olive *et al.*, *Review of particle physics*, Chin. Phys. **C38** (2014) 090001.

[43] LHCb collaboration, A. A. Alves Jr. *et al.*, *The LHCb detector at the LHC*, JINST **3** (2008) S08005.

[44] LHCb collaboration, R. Aaij *et al.*, *LHCb detector performance*, Int. J. Mod. Phys. **A30** (2015) 1530022, arXiv:1412.6352.

[45] R. Aaij *et al.*, *The LHCb trigger and its performance in 2011*, JINST **8** (2013) P04022, arXiv:1211.3055.

[46] I. Belyaev *et al.*, *Handling of the generation of primary events in* Gauss*, the LHCb simulation framework*, J. Phys. Conf. Ser. **331** (2011) 032047.

[47] T. Sjöstrand, S. Mrenna, and P. Skands, Pythia *6.4 physics and manual*, JHEP **05** (2006) 026, arXiv:hep-ph/0603175.

[48] D. J. Lange, *The EvtGen particle decay simulation package*, Nucl. Instrum. Meth. **A462** (2001) 152.

[49] P. Golonka and Z. Was, Photos *Monte Carlo: A precision tool for QED corrections in* Z *and* W *decays*, Eur. Phys. J. **C45** (2006) 97, arXiv:hep-ph/0506026.

[50] Geant4 collaboration, J. Allison *et al.*, Geant4 *developments and applications*, IEEE Trans. Nucl. Sci. **53** (2006) 270.

[51] Geant4 collaboration, S. Agostinelli *et al.*, Geant4*: A simulation toolkit*, Nucl. Instrum. Meth. **A506** (2003) 250.

[52] M. Clemencic *et al.*, *The LHCb simulation application,* Gauss*: Design, evolution and experience*, J. Phys. Conf. Ser. **331** (2011) 032023.

[53] LHCb collaboration, R. Aaij *et al.*, *Observation of associated production of a* Z *boson with a* D *meson in the forward region*, JHEP **04** (2014) 091, arXiv:1401.3245.

[54] LHCb collaboration, R. Aaij *et al.*, *Measurement of the track reconstruction efficiency at LHCb*, JINST **10** (2015) P02007, arXiv:1408.1251.

[55] F. Archilli *et al.*, *Performance of the muon identification at LHCb*, JINST **8** (2013) P10020, arXiv:1306.0249.

[56] M. Adinolfi *et al.*, *Performance of the LHCb RICH detector at the LHC*, Eur. Phys. J. **C73** (2013) 2431, arXiv:1211.6759.

[57] W. D. Hulsbergen, *Decay chain fitting with a Kalman filter*, Nucl. Instrum. Meth. **A552** (2005) 566, arXiv:physics/0503191.

[58] T. Skwarnicki, *A study of the radiative cascade transitions between the* Υ' *and* Υ *resonances*, PhD thesis, Institute of Nuclear Physics, Krakow, 1986, DESY-F31-86-02.

[59] LHCb collaboration, R. Aaij *et al.*, *Measurement of* Υ *production in* pp *collisions at* $\sqrt{s} = 2.76\,\text{TeV}$, Eur. Phys. J. **C74** (2014) 2835, arXiv:1402.2539.

[60] BaBar collaboration, J. P. Lees *et al.*, *Branching fraction measurements of the color-suppressed decays* $\bar{\text{B}}^0 \to \text{D}^{(*)0}\pi^0$, $\text{D}^{(*)0}\eta$, $\text{D}^{(*)0}\omega$, *and* $\text{D}^{(*)0}\eta'$ *and measurement of the polarization in the decay* $\bar{\text{B}}^0 \to \text{D}^{*0}\omega$, Phys. Rev. **D84** (2011) 112007, Erratum ibid. **D87** (2013) 039901, arXiv:1107.5751.

[61] R. T. Farouki, *The Bernstein polynomial basis: A centennial retrospective*, Comput. Aided Geom. Des. **29** (2012) 379.

[62] S. S. Wilks, *The large-sample distribution of the likelihood ratio for testing composite hypotheses*, Annals Math. Statist. **9** (1938) 60.

[63] M. Pivk and F. R. Le Diberder, sPlot*: A statistical tool to unfold data distributions*, Nucl. Instrum. Meth. **A555** (2005) 356, arXiv:physics/0402083.

[64] LHCb collaboration, R. Aaij *et al.*, *Precision luminosity measurements at LHCb*, JINST **9** (2014) P12005, arXiv:1410.0149.

[65] M. Cacciari, M. Greco, and P. Nason, *The $p_{\rm T}$ spectrum in heavy flavor hadroproduction*, JHEP **05** (1998) 007, arXiv:hep-ph/9803400.

[66] M. Cacciari, S. Frixione, and P. Nason, *The $p_{\rm T}$ spectrum in heavy flavor photoproduction*, JHEP **03** (2001) 006, arXiv:hep-ph/0102134.

[67] M. Cacciari *et al.*, *Theoretical predictions for charm and bottom production at the LHC*, JHEP **10** (2012) 137, arXiv:1205.6344.

[68] LHCb collaboration, R. Aaij *et al.*, *Measurement of Υ production in pp collisions at $\sqrt{s} = 7$ TeV*, Eur. Phys. J. **C72** (2012) 2025, arXiv:1202.6579.

[69] LHCb collaboration, R. Aaij *et al.*, *Production of J/ψ and Υ mesons in pp collisions at $\sqrt{s} = 8$ TeV*, JHEP **06** (2013) 064, arXiv:1304.6977.

[70] CMS collaboration, S. Chatrchyan *et al.*, *Measurement of the Υ(1S), Υ(2S) and Υ(3S) polarizations in* pp *collisions at $\sqrt{s} = 7$* TeV, Phys. Rev. Lett. **110** (2013) 081802, arXiv:1209.2922.

[71] J. C. Collins and D. E. Soper, *Angular distribution of dileptons in high-energy hadron collisions*, Phys. Rev. **D16** (1977) 2219.

[72] S. P. Baranov. private communication.

[73] M. Gück, E. Reya and A. Vogt, *Dynamical parton distributions revisited*, Eur. Phys. J. **C5** (1998) 461, arXiv:hep-ph/9806404.

[74] A. van Hameren, R. Maciuła, and A. Szczurek, *Production of two charm quark-antiquark pairs in single-parton scattering within the $k_{\rm T}$-factorization approach*, Phys. Lett. **B748** (2015) 167, arXiv:1504.06490.

[75] D. Martínez Santos and F. Dupertuis, *Mass distributions marginalized over per-event errors*, Nucl. Instrum. Meth. **A764** (2014) 150, arXiv:1312.5000.

[76] LHCb collaboration, R. Aaij *et al.*, *Measurement of* J/ψ *production in* pp *collisions at $\sqrt{s} = 7$* TeV, Eur. Phys. J. **C71** (2011) 1645, arXiv:1103.0423.

[77] M. Ferro-Luzzi, *Proposal for an absolute luminosity determination in colliding beam experiments using vertex detection of beam-gas interactions*, Nucl. Instrum. Meth. **A553** (2005) 388.

[78] LHCb collaboration, R. Aaij *et al.*, *Absolute luminosity measurements with the LHCb detector at the LHC*, JINST **7** (2012) P01010, arXiv:1110.2866.

[79] C. Barschel, *Precision luminosity measurement at LHCb with beam-gas imaging*, PhD thesis, RWTH Aachen University, Aachen, 2014, CERN-THESIS-2013-301.

[80] LHCb collaboration, R. Aaij *et al.*, *Measurement of* $\sigma(\mathrm{pp} \to \mathrm{b\bar{b}X})$ *at* $\sqrt{s} = 7\,\mathrm{TeV}$ *in the forward region*, Phys. Lett. **B694** (2010) 209, arXiv:1009.2731.

[81] LHCb collaboration, R. Aaij *et al.*, *Prompt charm production in* pp *collisions at* $\sqrt{s} = 13\,\mathrm{TeV}$, arXiv:1510.01707, submitted to JHEP.

[82] Particle Data Group, C. Amsler *et al.*, *Fragmentation functions in* $\mathrm{e^+e^-}$ *annihilation and lepton-nucleon DIS,* in *Review of particle physics*, Phys. Lett. **B667** (2008) 1.

[83] CDF collaboration, F. Abe *et al.*, *Study of four jet events and evidence for double parton interactions in* $\mathrm{p\bar{p}}$ *collisions at* $\sqrt{s} = 1.8\,\mathrm{TeV}$, Phys. Rev. **D47** (1993) 4857.

[84] D0 collaboration, V. M. Abazov *et al.*, *Double parton interactions in* γ*+3 jet events in* $\mathrm{p\bar{p}}$ *collisions at* $\sqrt{s} = 1.96\,\mathrm{TeV}$, Phys. Rev. **D81** (2010) 052012, arXiv:0912.5104.

[85] ATLAS collaboration, G. Aad *et al.*, *Measurement of hard double-parton interactions in* $\mathrm{W}(\to \ell\nu)$*+2 jet events at* $\sqrt{s} = 7\,\mathrm{TeV}$ *with the ATLAS detector*, New J. Phys. **15** (2013) 033038, arXiv:1301.6872.

[86] CMS collaboration, S. Chatrchyan *et al.*, *Study of double parton scattering using* W*+2-jet events in proton-proton collisions at* $\sqrt{s} = 7\,\mathrm{TeV}$, JHEP **03** (2014) 032, arXiv:1312.5729.

[87] D0 collaboration, V. M. Abazov *et al.*, *Double parton interactions in* $\gamma + 3$ *jet and* $\gamma + \mathrm{b/c}$ *jet* $+ 2$ *jet events in* $\mathrm{p\bar{p}}$ *collisions at* $\sqrt{s} = 1.96\,\mathrm{TeV}$, Phys. Rev. **D89** (2014) 072006.

[88] R. Astalos *et al.*, *Proceedings of the* 6^{th} *International Workshop on Multiple Partonic Interactions at the LHC*, arXiv:1506.05829.

[89] LHCb collaboration, R. Aaij *et al.*, *Opposite-side flavour tagging of* B *mesons at the LHCb experiment*, Eur. Phys. J. **C72** (2012) 2022, arXiv:1202.4979.

[90] LHCb collaboration, *Optimization and calibration of the same-side kaon tagging algorithm using hadronic* $\mathrm{B_s^0}$ *decays in 2011 data*, LHCb-CONF-2012-033.

[91] LHCb collaboration, *Performance of flavor tagging algorithms optimised for the analysis of* $\mathrm{B_s^0} \to \mathrm{J/\psi\,\phi}$, LHCb-CONF-2012-026.

[92] LHCb collaboration, R. Aaij *et al.*, *B flavour tagging using charm decays at the LHCb experiment*, JINST **10** (2015) P10005, arXiv:1507.07892.

LHCb collaboration

R. Aaij[38], C. Abellán Beteta[40], B. Adeva[37], M. Adinolfi[46], A. Affolder[52], Z. Ajaltouni[5], S. Akar[6], J. Albrecht[9], F. Alessio[38], M. Alexander[51], S. Ali[41], G. Alkhazov[30], P. Alvarez Cartelle[53], A.A. Alves Jr[57], S. Amato[2], S. Amerio[22], Y. Amhis[7], L. An[3], L. Anderlini[17], J. Anderson[40], G. Andreassi[39], M. Andreotti[16,f], J.E. Andrews[58], R.B. Appleby[54], O. Aquines Gutierrez[10], F. Archilli[38], P. d'Argent[11], A. Artamonov[35], M. Artuso[59], E. Aslanides[6], G. Auriemma[25,m], M. Baalouch[5], S. Bachmann[11], J.J. Back[48], A. Badalov[36], C. Baesso[60], W. Baldini[16,38], R.J. Barlow[54], C. Barschel[38], S. Barsuk[7], W. Barter[38], V. Batozskaya[28], V. Battista[39], A. Bay[39], L. Beaucourt[4], J. Beddow[51], F. Bedeschi[23], I. Bediaga[1], L.J. Bel[41], V. Bellee[39], N. Belloli[20,j], I. Belyaev[31], E. Ben-Haim[8], G. Bencivenni[18], S. Benson[38], J. Benton[46], A. Berezhnoy[32], R. Bernet[40], A. Bertolin[22], M.-O. Bettler[38], M. van Beuzekom[41], A. Bien[11], S. Bifani[45], P. Billoir[8], T. Bird[54], A. Birnkraut[9], A. Bizzeti[17,h], T. Blake[48], F. Blanc[39], J. Blouw[10], S. Blusk[59], V. Bocci[25], A. Bondar[34], N. Bondar[30,38], W. Bonivento[15], S. Borghi[54], M. Borisyak[65], M. Borsato[7], T.J.V. Bowcock[52], E. Bowen[40], C. Bozzi[16,38], S. Braun[11], M. Britsch[11], T. Britton[59], J. Brodzicka[54], N.H. Brook[46], E. Buchanan[46], C. Burr[54], A. Bursche[40], J. Buytaert[38], S. Cadeddu[15], R. Calabrese[16,f], M. Calvi[20,j], M. Calvo Gomez[36,o], P. Campana[18], D. Campora Perez[38], L. Capriotti[54], A. Carbone[14,d], G. Carboni[24,k], R. Cardinale[19,i], A. Cardini[15], P. Carniti[20,j], L. Carson[50], K. Carvalho Akiba[2,38], G. Casse[52], L. Cassina[20,j], L. Castillo Garcia[39], M. Cattaneo[38], Ch. Cauet[9], G. Cavallero[19], R. Cenci[23,s], M. Charles[8], Ph. Charpentier[38], M. Chefdeville[4], S. Chen[54], S.-F. Cheung[55], N. Chiapolini[40], M. Chrzaszcz[40], X. Cid Vidal[38], G. Ciezarek[41], P.E.L. Clarke[50], M. Clemencic[38], H.V. Cliff[47], J. Closier[38], V. Coco[38], J. Cogan[6], E. Cogneras[5], V. Cogoni[15,e], L. Cojocariu[29], G. Collazuol[22], P. Collins[38], A. Comerma-Montells[11], A. Contu[15], A. Cook[46], M. Coombes[46], S. Coquereau[8], G. Corti[38], M. Corvo[16,f], B. Couturier[38], G.A. Cowan[50], D.C. Craik[48], A. Crocombe[48], M. Cruz Torres[60], S. Cunliffe[53], R. Currie[53], C. D'Ambrosio[38], E. Dall'Occo[41], J. Dalseno[46], P.N.Y. David[41], A. Davis[57], O. De Aguiar Francisco[2], K. De Bruyn[6], S. De Capua[54], M. De Cian[11], J.M. De Miranda[1], L. De Paula[2], P. De Simone[18], C.-T. Dean[51], D. Decamp[4], M. Deckenhoff[9], L. Del Buono[8], N. Déléage[4], M. Demmer[9], D. Derkach[65], O. Deschamps[5], F. Dettori[38], B. Dey[21], A. Di Canto[38], F. Di Ruscio[24], H. Dijkstra[38], S. Donleavy[52], F. Dordei[11], M. Dorigo[39], A. Dosil Suárez[37], D. Dossett[48], A. Dovbnya[43], K. Dreimanis[52], L. Dufour[41], G. Dujany[54], P. Durante[38], R. Dzhelyadin[35], A. Dziurda[26], A. Dzyuba[30], S. Easo[49,38], U. Egede[53], V. Egorychev[31], S. Eidelman[34], S. Eisenhardt[50], U. Eitschberger[9], R. Ekelhof[9], L. Eklund[51], I. El Rifai[5], Ch. Elsasser[40], S. Ely[59], S. Esen[11], H.M. Evans[47], T. Evans[55], A. Falabella[14], C. Färber[38], N. Farley[45], S. Farry[52], R. Fay[52], D. Ferguson[50], V. Fernandez Albor[37], F. Ferrari[14], F. Ferreira Rodrigues[1], M. Ferro-Luzzi[38], S. Filippov[33], M. Fiore[16,38,f], M. Fiorini[16,f], M. Firlej[27], C. Fitzpatrick[39], T. Fiutowski[27], K. Fohl[38], P. Fol[53], M. Fontana[15], F. Fontanelli[19,i], D. C. Forshaw[59], R. Forty[38], M. Frank[38], C. Frei[38], M. Frosini[17], J. Fu[21], E. Furfaro[24,k], A. Gallas Torreira[37], D. Galli[14,d], S. Gallorini[22], S. Gambetta[50], M. Gandelman[2], P. Gandini[55], Y. Gao[3], J. García Pardiñas[37], J. Garra Tico[47], L. Garrido[36], D. Gascon[36], C. Gaspar[38], R. Gauld[55], L. Gavardi[9], G. Gazzoni[5], D. Gerick[11], E. Gersabeck[11], M. Gersabeck[54], T. Gershon[48], Ph. Ghez[4], S. Gianì[39], V. Gibson[47], O.G. Girard[39], L. Giubega[29], V.V. Gligorov[38], C. Göbel[60], D. Golubkov[31], A. Golutvin[53,38], A. Gomes[1,a], C. Gotti[20,j], M. Grabalosa Gándara[5], R. Graciani Diaz[36], L.A. Granado Cardoso[38], E. Graugés[36], E. Graverini[40], G. Graziani[17], A. Grecu[29], E. Greening[55], S. Gregson[47], P. Griffith[45], L. Grillo[11], O. Grünberg[63], B. Gui[59], E. Gushchin[33], Yu. Guz[35,38], T. Gys[38], T. Hadavizadeh[55], C. Hadjivasiliou[59], G. Haefeli[39],

C. Haen[38], S.C. Haines[47], S. Hall[53], B. Hamilton[58], X. Han[11], S. Hansmann-Menzemer[11], N. Harnew[55], S.T. Harnew[46], J. Harrison[54], J. He[38], T. Head[39], V. Heijne[41], K. Hennessy[52], P. Henrard[5], L. Henry[8], E. van Herwijnen[38], M. Heß[63], A. Hicheur[2], D. Hill[55], M. Hoballah[5], C. Hombach[54], W. Hulsbergen[41], T. Humair[53], N. Hussain[55], D. Hutchcroft[52], D. Hynds[51], M. Idzik[27], P. Ilten[56], R. Jacobsson[38], A. Jaeger[11], J. Jalocha[55], E. Jans[41], A. Jawahery[58], M. John[55], D. Johnson[38], C.R. Jones[47], C. Joram[38], B. Jost[38], N. Jurik[59], S. Kandybei[43], W. Kanso[6], M. Karacson[38], T.M. Karbach[38,†], S. Karodia[51], M. Kecke[11], M. Kelsey[59], I.R. Kenyon[45], M. Kenzie[38], T. Ketel[42], E. Khairullin[65], B. Khanji[20,38,j], C. Khurewathanakul[39], S. Klaver[54], K. Klimaszewski[28], O. Kochebina[7], M. Kolpin[11], I. Komarov[39], R.F. Koopman[42], P. Koppenburg[41,38], M. Kozeiha[5], L. Kravchuk[33], K. Kreplin[11], M. Kreps[48], G. Krocker[11], P. Krokovny[34], F. Kruse[9], W. Krzemien[28], W. Kucewicz[26,n], M. Kucharczyk[26], V. Kudryavtsev[34], A. K. Kuonen[39], K. Kurek[28], T. Kvaratskheliya[31], D. Lacarrere[38], G. Lafferty[54,38], A. Lai[15], D. Lambert[50], G. Lanfranchi[18], C. Langenbruch[48], B. Langhans[38], T. Latham[48], C. Lazzeroni[45], R. Le Gac[6], J. van Leerdam[41], J.-P. Lees[4], R. Lefèvre[5], A. Leflat[32,38], J. Lefrançois[7], E. Lemos Cid[37], O. Leroy[6], T. Lesiak[26], B. Leverington[11], Y. Li[7], T. Likhomanenko[65,64], M. Liles[52], R. Lindner[38], C. Linn[38], F. Lionetto[40], B. Liu[15], X. Liu[3], D. Loh[48], I. Longstaff[51], J.H. Lopes[2], D. Lucchesi[22,q], M. Lucio Martinez[37], H. Luo[50], A. Lupato[22], E. Luppi[16,f], O. Lupton[55], A. Lusiani[23], F. Machefert[7], F. Maciuc[29], O. Maev[30], K. Maguire[54], S. Malde[55], A. Malinin[64], G. Manca[7], G. Mancinelli[6], P. Manning[59], A. Mapelli[38], J. Maratas[5], J.F. Marchand[4], U. Marconi[14], C. Marin Benito[36], P. Marino[23,38,s], J. Marks[11], G. Martellotti[25], M. Martin[6], M. Martinelli[39], D. Martinez Santos[37], F. Martinez Vidal[66], D. Martins Tostes[2], A. Massafferri[1], R. Matev[38], A. Mathad[48], Z. Mathe[38], C. Matteuzzi[20], A. Mauri[40], B. Maurin[39], A. Mazurov[45], M. McCann[53], J. McCarthy[45], A. McNab[54], R. McNulty[12], B. Meadows[57], F. Meier[9], M. Meissner[11], D. Melnychuk[28], M. Merk[41], E Michielin[22], D.A. Milanes[62], M.-N. Minard[4], D.S. Mitzel[11], J. Molina Rodriguez[60], I.A. Monroy[62], S. Monteil[5], M. Morandin[22], P. Morawski[27], A. Mordà[6], M.J. Morello[23,s], J. Moron[27], A.B. Morris[50], R. Mountain[59], F. Muheim[50], D. Müller[54], J. Müller[9], K. Müller[40], V. Müller[9], M. Mussini[14], B. Muster[39], P. Naik[46], T. Nakada[39], R. Nandakumar[49], A. Nandi[55], I. Nasteva[2], M. Needham[50], N. Neri[21], S. Neubert[11], N. Neufeld[38], M. Neuner[11], A.D. Nguyen[39], T.D. Nguyen[39], C. Nguyen-Mau[39,p], V. Niess[5], R. Niet[9], N. Nikitin[32], T. Nikodem[11], A. Novoselov[35], D.P. O'Hanlon[48], A. Oblakowska-Mucha[27], V. Obraztsov[35], S. Ogilvy[51], O. Okhrimenko[44], R. Oldeman[15,e], C.J.G. Onderwater[67], B. Osorio Rodrigues[1], J.M. Otalora Goicochea[2], A. Otto[38], P. Owen[53], A. Oyanguren[66], A. Palano[13,c], F. Palombo[21,t], M. Palutan[18], J. Panman[38], A. Papanestis[49], M. Pappagallo[51], L.L. Pappalardo[16,f], C. Pappenheimer[57], W. Parker[58], C. Parkes[54], G. Passaleva[17], G.D. Patel[52], M. Patel[53], C. Patrignani[19,i], A. Pearce[54,49], A. Pellegrino[41], G. Penso[25,l], M. Pepe Altarelli[38], S. Perazzini[14,d], P. Perret[5], L. Pescatore[45], K. Petridis[46], A. Petrolini[19,i], M. Petruzzo[21], E. Picatoste Olloqui[36], B. Pietrzyk[4], T. Pilař[48], D. Pinci[25], A. Pistone[19], A. Piucci[11], S. Playfer[50], M. Plo Casasus[37], T. Poikela[38], F. Polci[8], A. Poluektov[48,34], I. Polyakov[31], E. Polycarpo[2], A. Popov[35], D. Popov[10,38], B. Popovici[29], C. Potterat[2], E. Price[46], J.D. Price[52], J. Prisciandaro[37], A. Pritchard[52], C. Prouve[46], V. Pugatch[44], A. Puig Navarro[39], G. Punzi[23,r], W. Qian[4], R. Quagliani[7,46], B. Rachwal[26], J.H. Rademacker[46], M. Rama[23], M. Ramos Pernas[37], M.S. Rangel[2], I. Raniuk[43], N. Rauschmayr[38], G. Raven[42], F. Redi[53], S. Reichert[54], M.M. Reid[48], A.C. dos Reis[1], S. Ricciardi[49], S. Richards[46], M. Rihl[38], K. Rinnert[52,38], V. Rives Molina[36], P. Robbe[7,38], A.B. Rodrigues[1], E. Rodrigues[54], J.A. Rodriguez Lopez[62], P. Rodriguez Perez[54], S. Roiser[38], V. Romanovsky[35], A. Romero Vidal[37], J. W. Ronayne[12], M. Rotondo[22], T. Ruf[38],

P. Ruiz Valls[66], J.J. Saborido Silva[37], N. Sagidova[30], P. Sail[51], B. Saitta[15,e], V. Salustino Guimaraes[2], C. Sanchez Mayordomo[66], B. Sanmartin Sedes[37], R. Santacesaria[25], C. Santamarina Rios[37], M. Santimaria[18], E. Santovetti[24,k], A. Sarti[18,l], C. Satriano[25,m], A. Satta[24], D.M. Saunders[46], D. Savrina[31,32], M. Schiller[38], H. Schindler[38], M. Schlupp[9], M. Schmelling[10], T. Schmelzer[9], B. Schmidt[38], O. Schneider[39], A. Schopper[38], M. Schubiger[39], M.-H. Schune[7], R. Schwemmer[38], B. Sciascia[18], A. Sciubba[25,l], A. Semennikov[31], N. Serra[40], J. Serrano[6], L. Sestini[22], P. Seyfert[20], M. Shapkin[35], I. Shapoval[16,43,f], Y. Shcheglov[30], T. Shears[52], L. Shekhtman[34], V. Shevchenko[64], A. Shires[9], B.G. Siddi[16], R. Silva Coutinho[40], L. Silva de Oliveira[2], G. Simi[22], M. Sirendi[47], N. Skidmore[46], T. Skwarnicki[59], E. Smith[55,49], E. Smith[53], I.T. Smith[50], J. Smith[47], M. Smith[54], H. Snoek[41], M.D. Sokoloff[57,38], F.J.P. Soler[51], F. Soomro[39], D. Souza[46], B. Souza De Paula[2], B. Spaan[9], P. Spradlin[51], S. Sridharan[38], F. Stagni[38], M. Stahl[11], S. Stahl[38], S. Stefkova[53], O. Steinkamp[40], O. Stenyakin[35], S. Stevenson[55], S. Stoica[29], S. Stone[59], B. Storaci[40], S. Stracka[23,s], M. Straticiuc[29], U. Straumann[40], L. Sun[57], W. Sutcliffe[53], K. Swientek[27], S. Swientek[9], V. Syropoulos[42], M. Szczekowski[28], T. Szumlak[27], S. T'Jampens[4], A. Tayduganov[6], T. Tekampe[9], M. Teklishyn[7], G. Tellarini[16,f], F. Teubert[38], C. Thomas[55], E. Thomas[38], J. van Tilburg[41], V. Tisserand[4], M. Tobin[39], J. Todd[57], S. Tolk[42], L. Tomassetti[16,f], D. Tonelli[38], S. Topp-Joergensen[55], N. Torr[55], E. Tournefier[4], S. Tourneur[39], K. Trabelsi[39], M.T. Tran[39], M. Tresch[40], A. Trisovic[38], A. Tsaregorodtsev[6], P. Tsopelas[41], N. Tuning[41,38], A. Ukleja[28], A. Ustyuzhanin[65,64], U. Uwer[11], C. Vacca[15,38,e], V. Vagnoni[14], G. Valenti[14], A. Vallier[7], R. Vazquez Gomez[18], P. Vazquez Regueiro[37], C. Vázquez Sierra[37], S. Vecchi[16], J.J. Velthuis[46], M. Veltri[17,g], G. Veneziano[39], M. Vesterinen[11], B. Viaud[7], D. Vieira[2], M. Vieites Diaz[37], X. Vilasis-Cardona[36,o], V. Volkov[32], A. Vollhardt[40], D. Volyanskyy[10], D. Voong[46], A. Vorobyev[30], V. Vorobyev[34], C. Voß[63], J.A. de Vries[41], R. Waldi[63], C. Wallace[48], R. Wallace[12], J. Walsh[23], S. Wandernoth[11], J. Wang[59], D.R. Ward[47], N.K. Watson[45], D. Websdale[53], A. Weiden[40], M. Whitehead[48], G. Wilkinson[55,38], M. Wilkinson[59], M. Williams[38], M.P. Williams[45], M. Williams[56], T. Williams[45], F.F. Wilson[49], J. Wimberley[58], J. Wishahi[9], W. Wislicki[28], M. Witek[26], G. Wormser[7], S.A. Wotton[47], S. Wright[47], K. Wyllie[38], Y. Xie[61], Z. Xu[39], Z. Yang[3], J. Yu[61], X. Yuan[34], O. Yushchenko[35], M. Zangoli[14], M. Zavertyaev[10,b], L. Zhang[3], Y. Zhang[3], A. Zhelezov[11], A. Zhokhov[31], L. Zhong[3], S. Zucchelli[14].

[1] *Centro Brasileiro de Pesquisas Físicas (CBPF), Rio de Janeiro, Brazil*
[2] *Universidade Federal do Rio de Janeiro (UFRJ), Rio de Janeiro, Brazil*
[3] *Center for High Energy Physics, Tsinghua University, Beijing, China*
[4] *LAPP, Université Savoie Mont-Blanc, CNRS/IN2P3, Annecy-Le-Vieux, France*
[5] *Clermont Université, Université Blaise Pascal, CNRS/IN2P3, LPC, Clermont-Ferrand, France*
[6] *CPPM, Aix-Marseille Université, CNRS/IN2P3, Marseille, France*
[7] *LAL, Université Paris-Sud, CNRS/IN2P3, Orsay, France*
[8] *LPNHE, Université Pierre et Marie Curie, Université Paris Diderot, CNRS/IN2P3, Paris, France*
[9] *Fakultät Physik, Technische Universität Dortmund, Dortmund, Germany*
[10] *Max-Planck-Institut für Kernphysik (MPIK), Heidelberg, Germany*
[11] *Physikalisches Institut, Ruprecht-Karls-Universität Heidelberg, Heidelberg, Germany*
[12] *School of Physics, University College Dublin, Dublin, Ireland*
[13] *Sezione INFN di Bari, Bari, Italy*
[14] *Sezione INFN di Bologna, Bologna, Italy*
[15] *Sezione INFN di Cagliari, Cagliari, Italy*
[16] *Sezione INFN di Ferrara, Ferrara, Italy*
[17] *Sezione INFN di Firenze, Firenze, Italy*

[18] *Laboratori Nazionali dell'INFN di Frascati, Frascati, Italy*
[19] *Sezione INFN di Genova, Genova, Italy*
[20] *Sezione INFN di Milano Bicocca, Milano, Italy*
[21] *Sezione INFN di Milano, Milano, Italy*
[22] *Sezione INFN di Padova, Padova, Italy*
[23] *Sezione INFN di Pisa, Pisa, Italy*
[24] *Sezione INFN di Roma Tor Vergata, Roma, Italy*
[25] *Sezione INFN di Roma La Sapienza, Roma, Italy*
[26] *Henryk Niewodniczanski Institute of Nuclear Physics Polish Academy of Sciences, Kraków, Poland*
[27] *AGH - University of Science and Technology, Faculty of Physics and Applied Computer Science, Kraków, Poland*
[28] *National Center for Nuclear Research (NCBJ), Warsaw, Poland*
[29] *Horia Hulubei National Institute of Physics and Nuclear Engineering, Bucharest-Magurele, Romania*
[30] *Petersburg Nuclear Physics Institute (PNPI), Gatchina, Russia*
[31] *Institute of Theoretical and Experimental Physics (ITEP), Moscow, Russia*
[32] *Institute of Nuclear Physics, Moscow State University (SINP MSU), Moscow, Russia*
[33] *Institute for Nuclear Research of the Russian Academy of Sciences (INR RAN), Moscow, Russia*
[34] *Budker Institute of Nuclear Physics (SB RAS) and Novosibirsk State University, Novosibirsk, Russia*
[35] *Institute for High Energy Physics (IHEP), Protvino, Russia*
[36] *Universitat de Barcelona, Barcelona, Spain*
[37] *Universidad de Santiago de Compostela, Santiago de Compostela, Spain*
[38] *European Organization for Nuclear Research (CERN), Geneva, Switzerland*
[39] *Ecole Polytechnique Fédérale de Lausanne (EPFL), Lausanne, Switzerland*
[40] *Physik-Institut, Universität Zürich, Zürich, Switzerland*
[41] *Nikhef National Institute for Subatomic Physics, Amsterdam, The Netherlands*
[42] *Nikhef National Institute for Subatomic Physics and VU University Amsterdam, Amsterdam, The Netherlands*
[43] *NSC Kharkiv Institute of Physics and Technology (NSC KIPT), Kharkiv, Ukraine*
[44] *Institute for Nuclear Research of the National Academy of Sciences (KINR), Kyiv, Ukraine*
[45] *University of Birmingham, Birmingham, United Kingdom*
[46] *H.H. Wills Physics Laboratory, University of Bristol, Bristol, United Kingdom*
[47] *Cavendish Laboratory, University of Cambridge, Cambridge, United Kingdom*
[48] *Department of Physics, University of Warwick, Coventry, United Kingdom*
[49] *STFC Rutherford Appleton Laboratory, Didcot, United Kingdom*
[50] *School of Physics and Astronomy, University of Edinburgh, Edinburgh, United Kingdom*
[51] *School of Physics and Astronomy, University of Glasgow, Glasgow, United Kingdom*
[52] *Oliver Lodge Laboratory, University of Liverpool, Liverpool, United Kingdom*
[53] *Imperial College London, London, United Kingdom*
[54] *School of Physics and Astronomy, University of Manchester, Manchester, United Kingdom*
[55] *Department of Physics, University of Oxford, Oxford, United Kingdom*
[56] *Massachusetts Institute of Technology, Cambridge, MA, United States*
[57] *University of Cincinnati, Cincinnati, OH, United States*
[58] *University of Maryland, College Park, MD, United States*
[59] *Syracuse University, Syracuse, NY, United States*
[60] *Pontifícia Universidade Católica do Rio de Janeiro (PUC-Rio), Rio de Janeiro, Brazil, associated to* [2]
[61] *Institute of Particle Physics, Central China Normal University, Wuhan, Hubei, China, associated to* [3]
[62] *Departamento de Fisica , Universidad Nacional de Colombia, Bogota, Colombia, associated to* [8]
[63] *Institut für Physik, Universität Rostock, Rostock, Germany, associated to* [11]
[64] *National Research Centre Kurchatov Institute, Moscow, Russia, associated to* [31]
[65] *Yandex School of Data Analysis, Moscow, Russia, associated to* [31]
[66] *Instituto de Fisica Corpuscular (IFIC), Universitat de Valencia-CSIC, Valencia, Spain, associated to* [36]
[67] *Van Swinderen Institute, University of Groningen, Groningen, The Netherlands, associated to* [41]

[a] *Universidade Federal do Triângulo Mineiro (UFTM), Uberaba-MG, Brazil*
[b] *P.N. Lebedev Physical Institute, Russian Academy of Science (LPI RAS), Moscow, Russia*
[c] *Università di Bari, Bari, Italy*
[d] *Università di Bologna, Bologna, Italy*
[e] *Università di Cagliari, Cagliari, Italy*
[f] *Università di Ferrara, Ferrara, Italy*
[g] *Università di Urbino, Urbino, Italy*
[h] *Università di Modena e Reggio Emilia, Modena, Italy*
[i] *Università di Genova, Genova, Italy*
[j] *Università di Milano Bicocca, Milano, Italy*
[k] *Università di Roma Tor Vergata, Roma, Italy*
[l] *Università di Roma La Sapienza, Roma, Italy*
[m] *Università della Basilicata, Potenza, Italy*
[n] *AGH - University of Science and Technology, Faculty of Computer Science, Electronics and Telecommunications, Kraków, Poland*
[o] *LIFAELS, La Salle, Universitat Ramon Llull, Barcelona, Spain*
[p] *Hanoi University of Science, Hanoi, Viet Nam*
[q] *Università di Padova, Padova, Italy*
[r] *Università di Pisa, Pisa, Italy*
[s] *Scuola Normale Superiore, Pisa, Italy*
[t] *Università degli Studi di Milano, Milano, Italy*

[†] *Deceased*